Experimental Mechanics
DOI 10.1007/s11340-012-9629-x

Piezonuclear Fission Reactions from Earthquakes and Brittle Rocks Failure: Evidence of Neutron Emission and Non-Radioactive Product Elements

A. Carpinteri · G. Lacidogna · A. Manuello · O. Borla

Received: 3 November 2011 / Accepted: 17 May 2012

Abstract Neutron emission measurements, by means of He^3 devices and bubble detectors, were performed during three different kinds of compression tests on brittle rocks: (i) under monotonic displacement control, (ii) under cyclic loading, and (iii) by ultrasonic vibration. The material used for the tests was Luserna stone, with different specimen sizes and shapes, and consequently with different brittleness numbers. Some studies had been already conducted on the different forms of energy emitted during the failure of brittle materials. They are based on the signals captured by acoustic emission measurement systems, or on the detection of electromagnetic charge. On the other hand, piezonuclear neutron emissions from very brittle rock specimens in compression have been discovered only very recently. In this paper, the authors analyse this phenomenon from an experimental point of view. Since the analyzed material contains iron, additional experiments have been performed on steel specimens subjected to tension and compression, observing, also in this case, neutron emissions well distinguishable from the background level. Our conjecture is that piezonuclear reactions involving fission of iron into aluminum, or into magnesium and silicon, should have occurred during compression damage and failure. This hypothesis is confirmed by the direct evidence of Energy Dispersive X-ray Spectroscopy (EDS) tests conducted on the specimens. It is also interesting to emphasize that the anomalous chemical balances of the major events that have affected the geomechanical and geochemical evolution of the Earth's Crust should be considered as an indirect evidence of the piezonuclear fission reactions considered above.

Keywords Neutron emissions · Piezonuclear reactions · Rocks crushing failure · Energy dispersive X-ray spectroscopy · Plate tectonics · Element evolution

A. Carpinteri (✉) · G. Lacidogna · A. Manuello · O. Borla
Department of Structural, Geotechnical and Building Engineering,
Politecnico di Torino,
Corso Duca degli Abruzzi 24,
10129 Torino, Italy
e-mail: alberto.carpinteri@polito.it

O. Borla
Istituto Nazionale di Fisica Nucleare, INFN sez. Torino,
Via Pietro Giuria 1,
10125 Torino, Italy

Introduction

This paper discusses the phenomenon of neutron emissions from brittle rock specimens under mechanical loading. The aim is to describe and demonstrate the neutron emissions from piezonuclear reactions that have been recently observed for the first time and published in [1–5], providing new experimental evidences.

The different forms of energy emitted during the failure of brittle materials have been mainly measured based on the signals captured by the acoustic emission (AE) measurement systems [6–15], or on the detection of the electromagnetic (EM) charge [16–23]. The AE technique analyses the transient elastic waves due to stress redistribution following fracture propagation. Different experiments in measuring the released energy from fracture of brittle rocks conducted by AE have been pioneering [6–8]. Nowadays, the AE technique is well-known in the scientific community and applied for monitoring purposes also to concrete structures [9]. In addition, based on the analogy between AE and seismic activity, AE associated with microcracks are monitored and power-law frequency vs. magnitude statistics are observed [10–15]. The EM signals are related to brittle materials in which the fracture propagation occurs suddenly

Published online: 29 June 2012

and it is accompanied by abrupt stress drops in the stress–strain curve. A number of laboratory studies revealed the existence of EM signals during fracture experiments carried out on a wide range of materials [16]. Moreover, it was observed that the EM signals detected during failure of materials are analogous to the anomalous radiation of geo-electromagnetic waves observed before major earthquakes [17], reinforcing the idea that the EM effect can be applied as a forecasting tool for seismic events. A relevant attempt to explain the EM emission origin is the assumption that it is caused by net charges of opposite sign appearing on the vibrating faces of opening fractures [18–21]. According to this model, the EME amplitude increases as long as fracture propagates, since the rupture of new atomic bonds contributes to the EME. When the fracture arrests, the AE waves and the EM signals decay by relaxation [22, 23].

As regards the neutron emissions, we present original experimental tests performed on brittle rock test specimens, using He^3 neutron detectors and bubble type BD thermodynamic neutron detectors. We carried out three different kinds of compression tests on natural non-radioactive rock: (i) under monotonic displacement control, (ii) under cyclic loading, and (iii) by ultrasonic vibrations. Similarly to the preliminary piezonuclear experiments presented in [1–3], the material used for the tests is non-radioactive Luserna stone.

In these new tests, cylindrical specimens with different size and slenderness are used instead of prismatic specimens as in the preliminary tests. The compression tests were performed at the Fracture Mechanics Laboratory of the Politecnico of Torino, while the ultrasonic tests at the Medical and Environmental Physics Laboratory of the University of Torino.

For the specimens of larger dimensions, neutron emissions, detected by He^3, were found to be of about one order of magnitude higher than the ordinary natural background level at the time of the catastrophic failure. As regards test specimens with more ductile behaviour, neutron emissions significantly higher than the background level were found. These emissions fully confirm the preliminary tests [1–5] and are due to piezonuclear reactions, which depend on the different modalities of energy release during the tests. For specimens with sufficiently large size and slenderness, a relatively high energy release is expected, and hence a higher probability of neutron emissions at the time of failure. Furthermore, during compression tests under cyclic loading, an equivalent neutron dose was found at the end of the test, by neutron bubble detectors, about twice higher than the ordinary background level. Finally, by using an ultrasonic horn suitably joined with the specimen, ultrasonic tests were carried out on Luserna stone specimens in order to produce continuing vibration at 20 kHz. At the end of the tests, an equivalent neutron dose about twice higher than the background level was found. The preliminary results of this study are reported in [4, 5]. Since the Luserna stone presents a certain iron concentration (~3 % of Fe2O3 as total Fe [24]) localized into two specific minerals (phengite and biotite), it was supposed that piezonuclear reactions involving fission of iron into aluminum, or into magnesium and silicon, should have occurred during compression of the specimens [1–3]. In the classical process of nuclear fission a neutron strikes a heavy nucleus that splits into two lighter fragments. Each of the two fragments consists of a nucleus with roughly half the neutrons and protons of the original nucleus. This fission process releases a large amount of energy and gamma rays are emitted as well as two or more neutrons that are no longer bounded to the fission fragments. These *free neutrons* are then capable of splitting other heavy nuclei, which then release neutrons that split again more nuclei.

On the other hand *piezonuclear fission reactions* consist in a new nuclear phenomenon, produced by new physical causes such as pressure, fracture or cavitation, and from which neutrons can be produced without gamma emission.

Therefore, to give further confirmations on the iron key role into piezonuclear experiments, additional tests have been conducted on steel specimens under tension and compression loading. Also in this case, neutron emissions greater than twice the background level were observed after the achievement of the ultimate strength.

The assumed fissions of iron into aluminium, or into magnesium and silicon, are also supported by spectroscopical analyses of the fracture surfaces and by consistent geological data [24, 25]. The results of Energy Dispersive X-ray Spectroscopy (EDS), performed on samples coming from the Luserna stone specimens used in the preliminary experiments [1–3], show that, on the fracture surfaces, a considerable reduction in the iron content (~25 %) is very consistently counterbalanced by an increase in Al, Si, and Mg concentrations [24].

Moreover, the present natural abundances of aluminum (~8 %), and silicon (28 %) and scarcity of iron (~4 %) in the continental Earth's crust are possibly due to the piezonuclear fission reactions considered above [25]. These reactions would be activated where the environment conditions (pressure and temperature) are particularly severe, and mechanical phenomena of fracture, crushing, fragmentation, comminution, erosion, friction, etc., may occur. If we consider the evolution of the percentages of the most abundant elements in the Earth crust during the last 4.5 billion years, we realize that iron and nickel have drastically diminished, whereas aluminum and silicon have as much increased. It is also interesting to realize that such increases have developed mainly in the tectonic regions, where frictional phenomena between the continental plates occurred [25–28].

Neutron Emission Detection Techniques

Since neutrons are electrically neutral particles, they cannot directly produce ionization in a detector, and therefore cannot be directly detected. This means that neutron detectors must rely upon a conversion process where an incident neutron interacts with a nucleus to produce a secondary charged particle. These charged particles are then detected, and from them the neutrons presence is deduced. For an accurate neutron evaluation, a He^3 proportional counter and a He^3 radiation monitor were used.

Due to the difficulties in neutron measurements with the presence of an electromagnetic field, electromagnetic emissions (EME) were also monitored during compression tests by using a measuring device with working frequency range from few Hz up to several MHz. The experimental results [29] show that the typical EME detected during the tests are included in the frequency range from 160 kHz to 4 MHz. The neutron detectors used are designed and manufactured under a quality system, in compliance with the standard requirements provided by the International Electrotechnical Commission for EMI (Electro-Magnetic Interference). In particular, the instruments used are insensitive to electromagnetic noise in the frequency range from 150 kHz to 230 MHz. Thanks to the good immunity to electromagnetic disturbances, no spurious counts were observed during the tests. Moreover, a set of passive neutron detectors, based on the superheated bubble detection technique and insensitive to electromagnetic noise, were employed.

He^3 Neutron Proportional Counter

The He^3 detector used in the compression tests under monotonic displacement control, and by ultrasonic vibration, is a He^3 type (Xeram, France) with electronics of preamplification, amplification, and discrimination directly connected to the detector tube. The detector is powered with 1.3 kV, supplied via a high voltage NIM (Nuclear Instrument Module). The logic output producing the TTL (transistor-transistor logic) pulses is connected to a NIM counter. The device was calibrated for the measurement of thermal neutrons; its sensitivity is 65 cps/$n_{thermal}$ (± 10 % declared by the factory) i.e., a thermal neutron flux of 1 thermal neutron/s cm^2 corresponds to a count rate of 65 cps.

Considering that the fracture of dielectric materials, such as rocks, can lead to the emission of charged and neutral particles (electrons, photons, hard X-rays), in order to avoid possible false neutron measurements the output of the detector is enabled for detecting signals only exceeding 300 mV. This threshold value was determined by measuring the analog signal of the detector by means of a Co-60 gamma source (half-life: 5.271 years, type decay: $beta^-$, beta maximum energy: 317.8 keV, gammas: 1173.2 keV and 1332.5 keV). The presence of an interfering capacity on the charge preamplifier input increases the electronic noise and consequently the probability of spurious counts. For this reason, the coaxial cable used for connecting detector and charge preamplifier presented a low capacity (36 pF/m) and a short length (about 50 cm). Moreover, during the experimental measurements, the front-end electronics was screened with aluminum foils, and the He^3 tube was immersed in a sound-absorbing substance such as polystyrene in order to avoid possible accidental impacts and vibrations.

Neutron Bubble Detectors

A set of passive neutron detectors insensitive to electromagnetic noise and with zero gamma sensitivity was used in compression tests under cyclic loading. The dosimeters, based on superheated bubble detectors (BTI, Ontario, Canada) (BUBBLE TECHNOLOGY INDUSTRIES (1992)) [30], are calibrated at the factory against an Am-Be source in terms of NCRP38 (NCRP report 38 (1971)) [31]. Bubble detectors provide instant visible detection and measurement of neutron dose. Each detector is composed of a polycarbonate vial filled with elastic tissue-equivalent polymer, in which droplets of a superheated gas (Freon) are dispersed. When a neutron strikes a droplet, the latter immediately vaporizes, forming a visible gas bubble trapped in the gel. The number of droplets provides a direct measurement of the equivalent neutron dose. These detectors are suitable for neutron integral dose measurements, in the energy ranges of thermal neutrons (E=0.025 eV) and fast neutrons (E>100 keV).

He^3 Neutron Radiation Monitor

A portable high-sensitive He^3 gas filled proportional counter to measure neutron radiation dose equivalent and dose equivalent rate was used in the ultrasonic vibration tests. The radiation monitor AT1117M (ATOMTEX, Minsk, Republic of Belarus) is a multifunctional portable instrument with a digital readout consisting of a processing unit (PU) with an internal Geiger-Müller tube and external smart probes (BDKN-03 type). This type of device provides a high sensitivity and wide measuring ranges (neutron energy range 0.025 eV–14 MeV), with a fast response to radiation field change. An absolute calibration was carried out at the factory and a further calibration has been performed at the Experimental Physics Department of University of Turin by exposing the detector to a 30 mCi Am-Be source with a neutron emission of about 6.5E4 n/s within the solid angle with a tolerance of 10 %. A BERTHOLD LB 6411 neutron dose rate probe was used in order to compare the results with the AT1117M ones. The measurements confirmed a good agreement within 8–10 %.

Compression Tests Under Monotonic Displacement Control

Preliminary Tests on Prismatic Specimens

Preliminary tests on prismatic specimens were presented in previous contributions, recently published [1–3], and related to piezonuclear reactions occurring in solids containing iron −samples of Luserna rocks− in compression. The materials selected for the compression tests were Carrara Marble (calcite) and Luserna stone (gneiss). This choice was prompted by the consideration that, test specimen dimensions being the same, different brittleness numbers [32] would cause catastrophic failure in granite, not in marble. The test specimens were subjected to uniaxial compression to assess scale effects on brittleness [33].

Four test specimens were used, two made of Carrara marble and two made of Luserna stone. All of them were of the same size and shape, measuring $6\times6\times10=360$ cm^3. A standard servo-hydraulic press with a maximum capacity of 500 kN, equipped with control electronics, was used in these preliminary tests. This machine makes it possible to carry out tests in either load control or displacement control. The tests were performed in piston travel displacement control by setting, for all the test specimens, a velocity of 0.001 mm/s during compression. Neutron emission measurements were made by means of a He^3 detector placed at a distance of 10 cm from the test specimen and enclosed in a polystyrene case, to prevent the results from being altered by impacts or vibrations.

The measurements of neutron emissions obtained on marble yielded values comparable with the background, even at the time of test specimen failure. The neutron measurements obtained on the two Luserna stone test specimens, instead, exceeded the background value by about one order of magnitude when catastrophic failure occurred. These phenomena were assumed to be caused by piezonuclear reactions, that occurred in the Luserna stone, but did not in the marble [1–3]. Moreover, granite contains iron, which appears to be the most favourable element for the production of piezonuclear reactions [34, 35]. These experimental evidences induced the authors to carry out further tests on cylindrical Luserna stone specimens of different size and shape.

Tests on Cylindrical Specimens: Experimental Set-Up

Neutron emissions were measured on nine Luserna stone cylindrical specimens, of different size and shape (Table 1, Fig. 1), denoted with P1, P2,…, P9 [4]. The tests were carried out by means of a servo-hydraulic press, with a maximum capacity of 1,800 kN, working by a digital type electronic control unit. The management software was TESTXPERTII by Zwick/Roel (Zwick/Roel Group, Ulm, Germany), while the mechanical parts are manufactured by Baldwin (Instron Industrial Products Group, Grove City, PA, USA). The force applied was determined by measuring the pressure in the loading cylinder by means of a transducer. The margin of error in the determination of the force is 1 %, which makes it a class 1 mechanical press. The specimens were arranged with the two smaller surfaces in contact with the press platens, without coupling materials in-between, according to the testing modalities known as “test by means of rigid platens with friction”. The platen was controlled by means of a wire-type potentiometric displacement transducer. The tests were performed under displacement control, with the planned displacement velocities ranging from 0.001 to 0.01 mm/s.

The He^3 neutron detector was switched on at least 1 h before the beginning of each compression test, in order to reach the thermal equilibrium of electronics, and to make sure that the behaviour of the device was stable with respect to intrinsic thermal effects. The detector was placed in front of the test specimen at a distance of 10 cm and it was

Table 1 Characteristics of displacement-controlled compression tests on Luserna stone specimens

Granite specimen	Geometry of the specimen			Displacement velocity (mm/s)	Peak load (kN)	Peak stress (MPa)	Time at the peak load (s)
	D (mm)	H (mm)	λ = H/D				
P1	28	14	0.5	0.001	52.19	84.8	735.0
P2	28	28	1	0.001	33.46	54.4	1239.0
P3	28	56	2	0.001	41.28	67.1	1089.0
P4	53	25	0.5	0.001	129.00	58.5	960.0
P5	53	50	1	0.001	139.10	63.0	2460.0
P6	53	101	2	0.001	206.50	93.6	1180.0
P7	112	60	0.5	0.01	1099.30	111.6	231.3
P8	112	112	1	0.01	1077.10	109.4	263.5
P9	112	224	2	0.01	897.80	91.2	218.6

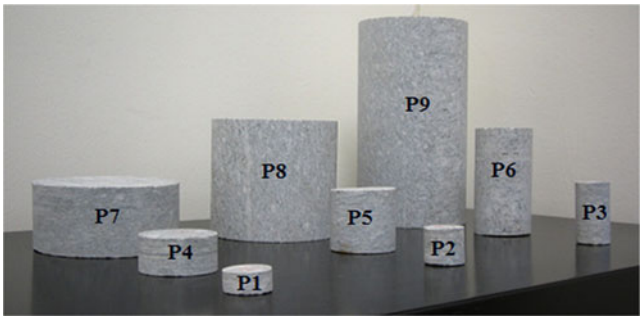

Fig. 1 Luserna stone cylindrical specimens, by varing slenderness and size-scale

enclosed in a polystyrene case in order to avoid "spurious" signals coming from impacts and vibrations.

A relative measurement of natural neutron background was performed in order to assess the average background affecting data acquisition in experimental room condition. The He^3 device was positioned in the same condition of the experimental set up and the background measures were performed fixing at 60 s the acquisition time, during a preliminary period of more than 3 h, for a total number of 200 counts. The average measured background level is ranging from $(3.17\pm0.32)\cdot10^{-2}$ to $(4.74\pm0.46)\cdot10^{-2}$ cps (see Table 2).

Tests on Cylindrical Specimens: Experimental Results

Additional background measurements were repeated before each test, fixing an acquisition time of 60 s in order to check a possible variation in natural background. Neutron measurements of specimen P2, P3, P4, P7 yielded values comparable with the ordinary natural background, whereas in specimens P1 and P5 the experimental data exceeded the background value by about four times. For specimen P6 neutron emissions of about five times the background level were observed concomitant with the sharp stress drop at the time of failure, while for specimens P8 and P9, the neutron emissions achieved values of about one order of magnitude higher than the ordinary background. In Figs. 2, 3 and 4 the load vs. time diagram, and the neutron count rate evolution for each specimen are shown. In Table 2, the experimental data concerning compression tests on the nine Luserna stone specimens are summarized.

The preliminary experimental results described above, and reported in [1–3], are confirmed by those obtained from compression tests on the cylindrical specimens. Neutron emissions related to specimens with very brittle or catastrophic failure result to be larger by about one order of magnitude than the ordinary background (see Figs. 3(c) and 4(b), (c)). Instead, in specimens with more ductile behaviour, neutron emissions were found to be only three or four times higher than the background level (see Figs. 2(a) and 3(b)).

The maximum neutron emissions were obtained from rock specimens exceeding a certain volume threshold: 360 cm^3 for the prismatic specimens, and 233 cm^3 for the cylindrical specimens. The experimental results show that a volume approximately exceeding 200 cm^3, combined with the extreme brittleness of the tested material, represents a threshold value for a neutron emission of about one order of magnitude higher than the ordinary background.

In addition, the experimental results seem to demonstrate that neutron emissions follow an anisotropic and impulsive distribution from a specific zone of the specimen. It is a matter of fact that the detected neutron flux, and consequently neutron dose, is inversely proportional to the square of the distance from the source. For these reasons, the He^3 device could have underestimated neutron flux intensity. A possible solution to avoid underestimated data acquisition is an experimental measurement by using more than one He^3 detector and more bubble dosimeters placed around the test specimen.

The main and peculiar characteristic of piezonuclear fission reactions is neutron production without gamma emission. This physical phenomenon is the signature of a new physics of nuclear interactions, as it is theoretically and

Table 2 Compression tests under monotonic displacement control. Neutron emissions experimental data on Luserna stone specimens

Granite specimen	D (mm)	λ = H/D	Average neutron background (10^{-2} cps)	Count rate at the neutron emission (10^{-2} cps)
P1	28	0.5	3.17±0.32	8.33±3.73
P2	28	1	3.17±0.32	background
P3	28	2	3.17±0.32	background
P4	53	0.5	3.83±0.37	background
P5	53	1	3.84±0.37	11.67±4.08
P6	53	2	4.74±0.46	25.00±6.01
P7	112	0.5	4.20±0.80	background
P8	112	1	4.20±0.80	30.00±11.10
P9	112	2	4.20±0.80	30.00±10.00

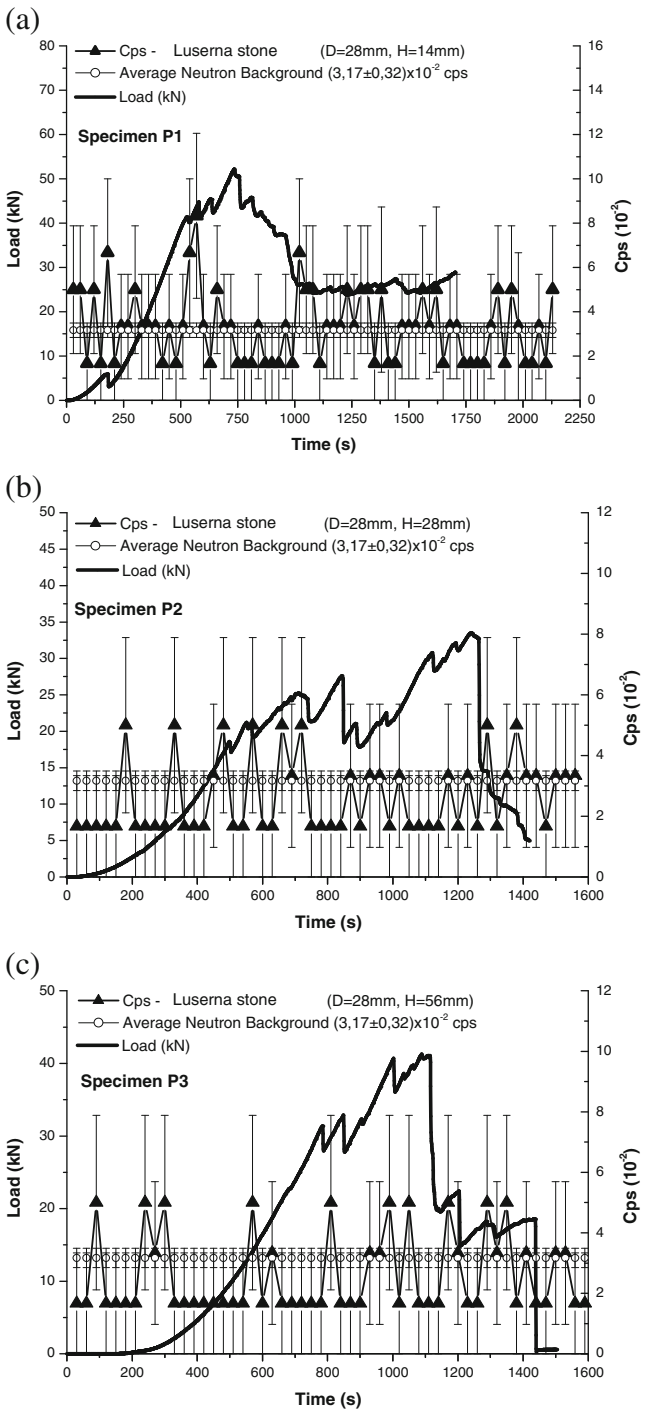

Fig. 2 Specimens P1, P2, P3. Load vs. time diagrams, and neutron emissions count rate

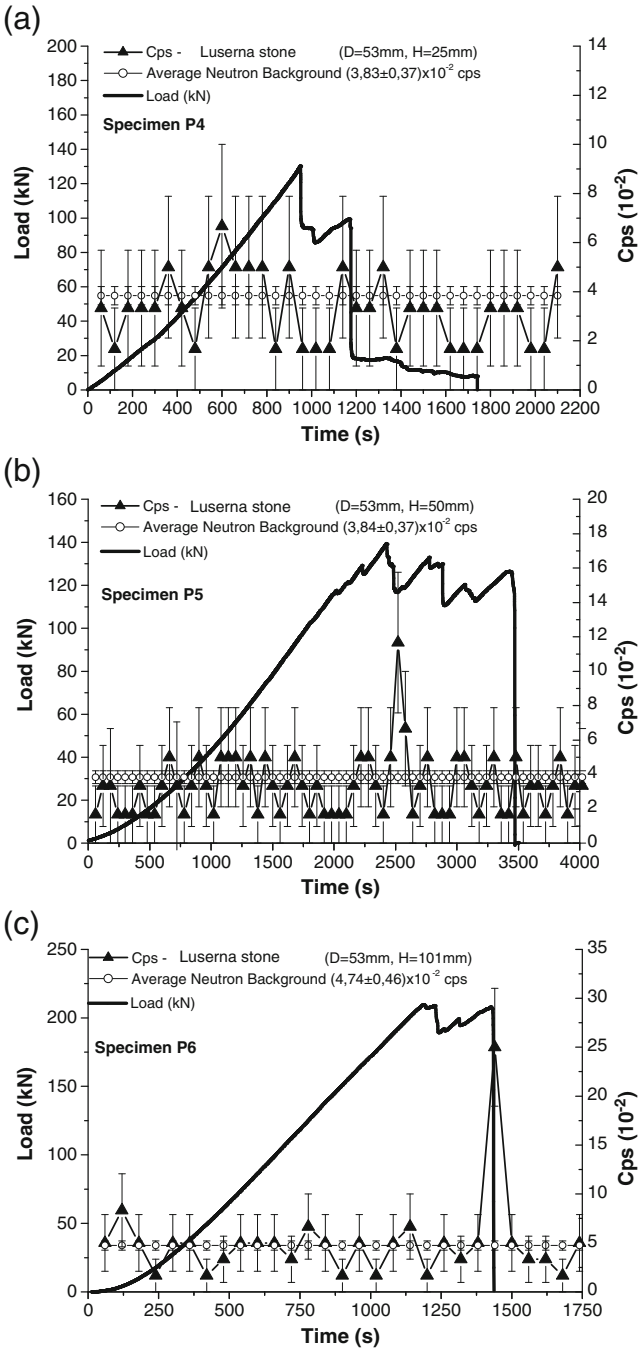

Fig. 3 Specimens P4, P5, P6. Load vs. time diagrams, and neutron emissions count rate

experimentally discussed in the literature [1–3, 34, 35]. Otherwise, we would have classical nuclear reactions (neutrons and gamma rays) produced by new methods such as pressure, fracture (solids), or cavitation (liquids). Instead, we are dealing with new low energy nuclear reactions (neutrons without gamma rays) produced by new methods as well.

Compression Tests Under Cyclic Loading

Experimental Set-Up

Neutron emissions from compression tests under cyclic loading were detected by using neutron bubble detectors. Due to their isotropic angular response, three BDT (Bubble Detector Thermal) and three BD-PND (Bubble Detector—Personal Neutron Dosimeter) detectors were positioned at a distance of about

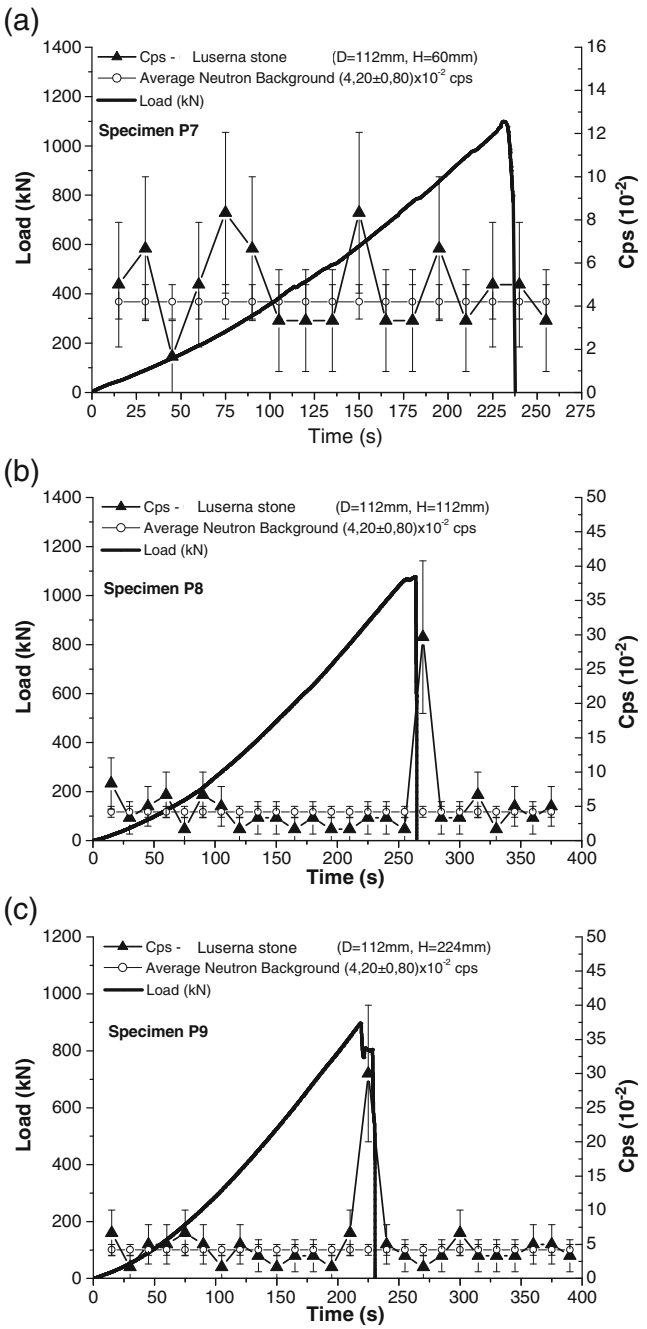

Fig. 4 Specimens P7, P8, P9. Load vs. time diagrams, and neutron emissions count rate

5 cm, all around the specimen. The detectors had been previously activated, unscrewing the protection cap, in order to reach the suitable thermal equilibrium, and they were kept active for all the test duration. Furthermore, a BDT and a BD-PND detector were used for the background control during the test. Three different tests were performed on Luserna stone specimens with the same shape and size (D=53 mm, H=53 mm, λ=1).

The cyclic loading was fixed at a frequency of 2 Hz for the three specimens. The load excursion was programmed respectively from a minimum load of 15 kN to a maximum of 110 kN during the first cyclic loading trial, from a minimum load of 12 kN to a maximum of 85 kN in the second test, and from a minimum of 10 kN to a maximum of 60 kN during the third test. Test durations were approximately of 1,126 min., 21 min., and 5,026 min., respectively. The experimental results are summarized in Table 3.

Experimental Results

Droplets counting was performed every 12 h and the equivalent neutron dose was calculated. In the same way, the natural background was estimated by means of the two bubble dosimeters used for assessment.

In the first test the background dose was found to be (26.32±5.26) nSv/h. A significant increment in the neutron emission with respect to the background level was detected at specimen failure. The equivalent neutron dose, at the end of the test, was (45.77±9.15) nSv/h.

The background associated to the second test was of (27.77±5.56) nSv/h. The neutron dose variation was found to be more than twice higher than the ordinary background, (59.29±11.86) nSv/h. In this test, bubbles were formed concurrently to specimen failure. Due to the very short duration of the test, droplets reading was always performed after 12 h, and compared with the natural background value. In this way it was possible to reduce experimental uncertainty related to equivalent neutron dose evaluation.

Finally, during the third test the ordinary background was found to be (13.98±2.76) nSv/h. The neutron equivalent dose variation, evaluated during the third cyclic loading test, is reported in Fig. 5 [4, 5]. Also in this case, an increment of more than twice with respect to the background level was detected at specimen failure. No significant variations in neutron emissions were observed before the failure. The equivalent neutron dose, at the end of the test, was (28.74±5.75) nSv/h (see also Table 3).

Table 3 Compression test under cyclic loading. Neutron emissions experimental data on Luserna gstone specimens

Test	Min – Max load (kN)	Test duration (min)	Average neutron background (nSv/h)	Equivalent neutron dose at the end of the test (nSv/h)	Equivalent neutron dose to neutron background ratio
1	15–110	1126	(26.32±5.26)	(45.77±9.15)	(1.74±0.35)
2	12–85	21	(27.77±5.56)	(59.29±11.86)	(2.14±0.43)
3	10–60	5026	(13.98±2.76)	(28.74±5.75)	(2.06±0.41)

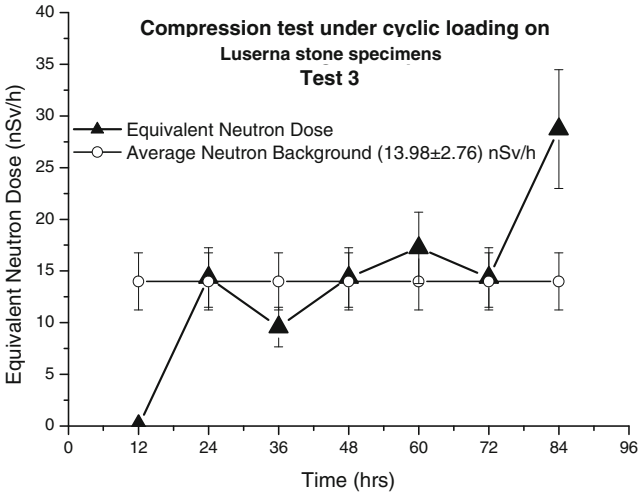

Fig. 5 Compression test under cyclic loading. Equivalent neutron dose variation during the third test on Luserna stone specimen

The comparison between background equivalent neutron dose and equivalent neutron dose at the end of the cyclic loading tests are reported in Fig. 6. From Table 3, considering the sensitivity of bubble detectors (20 %), it is possible to observe that in each test the average increment in equivalent neutron dose at failure is about twice higher than the natural neutron background.

Ultrasonic Tests

Experimental Set-Up

Ultrasonic oscillation was generated by an high intensity ultrasonic horn (Bandelin HD 2200) (see Fig. 7) working at 20 kHz [4, 5]. The device guarantees a constant amplitude

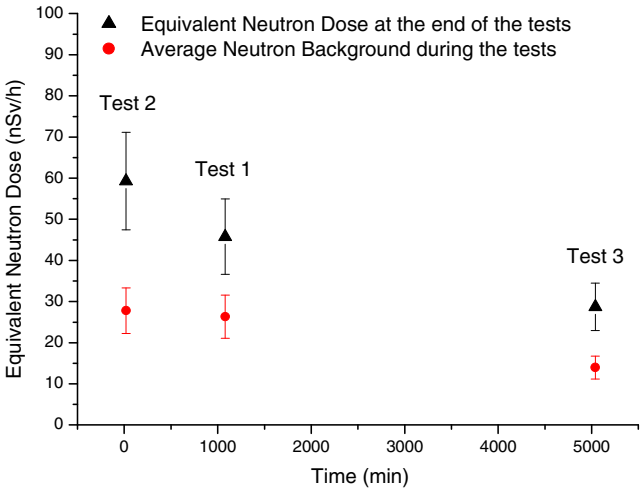

Fig. 6 Compression tests under cyclic loading. Comparison between the background equivalent neutron dose and the equivalent neutron dose at the end of the tests

Fig. 7 The Luserna stone specimen connected to the ultrasonic horn. The ultrasonic apparatus (Bandelin HD 2200) consists of a generator that converts electrical energy to 20 kHz ultrasound, and of a transducer that switches this energy into mechanical longitudinal vibration of the same frequency

(ranging from 10 % to 100 %) independently of changing conditions within the sample. The apparatus consists of a generator that converts electrical energy to 20 kHz ultrasounds, and of a transducer that switches this energy into mechanical longitudinal vibration at the same frequency.

The ultrasonic test on a Luserna stone specimen (D=53 mm, H=100 mm, λ=2) was carried out at the Medical and Environmental Physics Laboratory of Experimental Physics Department of the University of Torino [4, 5]. A relative natural background measurement was performed by means of the He^3 detector for more than 6 h. The average natural background was of $(6.50\pm0.85)\cdot10^{-3}$ cps, for a corresponding thermal neutron flux of $(1.00\pm0.13)\cdot10^{-4}$ $n_{thermal}cm^{-2}$ s^{-1}. This natural background level, lower than the one calculated during the compression tests at the Fracture Mechanics Laboratory of the Politecnico di Torino, is in agreement with the location of the Experimental Physics Laboratory, which is three floors below the ground level. A further estimation of neutron radiation dose equivalent was carried out by using a portable high-sensitive He^3 gas filled proportional counter (ATOMTEX, AT1117M). The device was switched on at least 2 h before the beginning of the test in order to reach suitable electronics temperature equilibrium and to perform a good evaluation of background. The average dose equivalent background was found to be (0.91±0.11) nSv/h.

Experimental Results

During the ultrasonic test, the specimen temperature was monitored by using a multimeter/thermometer (Tektronix

mod. S3910). The temperature reached 50 °C after 20 min, and then increased up to a maximum level around 100 °C at the end of the ultrasonic test. In Fig. 8, the neutron emissions detected are compared with the transducer power trend and the specimen temperature. A significant increment in neutron activity after 130 min from the beginning of the test was measured. At this time, the transducer power reached 30 % of the maximum, with a specimen temperature of about 90 °C. Some neutron variations were detected during the first hour of the test, but they could be due to ordinary fluctuations of natural background. At the switching off of the sonotrode, the neutron activity decreased to the typical background level.

A similar behavior in neutron variation was also detected by the Atomtex He^3 proportional counter. In Fig. 9, the neutron dose equivalent is compared with the neutron emission detected by Xeram He^3 device. A significant increment in neutron equivalent dose variation, at 120 min and 170 min, is observed in correspondence to the neutron emission variations in terms of cps. Also in this case, at the switching off of the sonotrode, the neutron activity decreased to the typical background level.

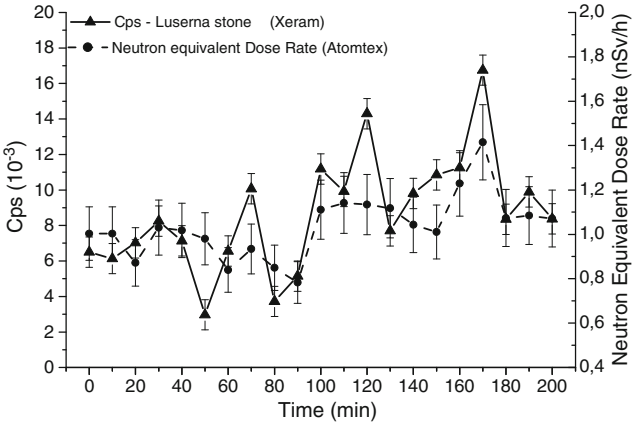

Fig. 9 Ultrasonic test. Neutron emissions (Xeram) compared with neutron equivalent dose rate variation (Atomtex)

Steel Specimens Under Tension and Compression Loading

Experimental Set-Up

Further specific tests have been conducted on two steel specimens, S_1 and S_2, subjected to tension and compression loading condition respectively. The two specimens, made of the same steel (FeB44k), present different heights and diameters. The first specimen (S_1), tested in tension, has diameter D=24 mm and length L=1,000 mm, the second specimen (S_2), tested in compression, has diameter D=40 mm and length L=50 mm. The specimen S_1 was subjected to tension up to failure according to EN ISO 6892 recommendation [36]. At the end of the test, a bar elongation of about 58 % of the initial length was obtained. The specimen S_2, instead, was subjected to compression loading up to obtain a final shortening of about 50 % of the initial length.

In Fig. 10(a) the test configuration for specimen S_1 is reported. To carry out these experiments, an hydraulic press, Walter Bai type, with electronic control was used. The test was conducted in three subsequent stages. In the first stage it was controlled by stress increments of 15 MPa/s up to the value of about 500 MPa, which corresponds to the yield stress of the material. Subsequently, the test was controlled by an imposed strain of 0.16 mm/s up to an elongation equal to 10 % of the initial length. In the last stage, which ended with the specimen failure (Fig. 10(b)), the imposed strain was applied by displacement increments of 0.33 mm/s. In Table 4, the applied loads, as well as the geometrical and mechanical characteristics of the specimens are summarized.

The compression test on specimen S_2 was performed under loading control using an hydraulic press, Galdabini type, with a maximum load of 5,000 kN (Fig 11(a)). A

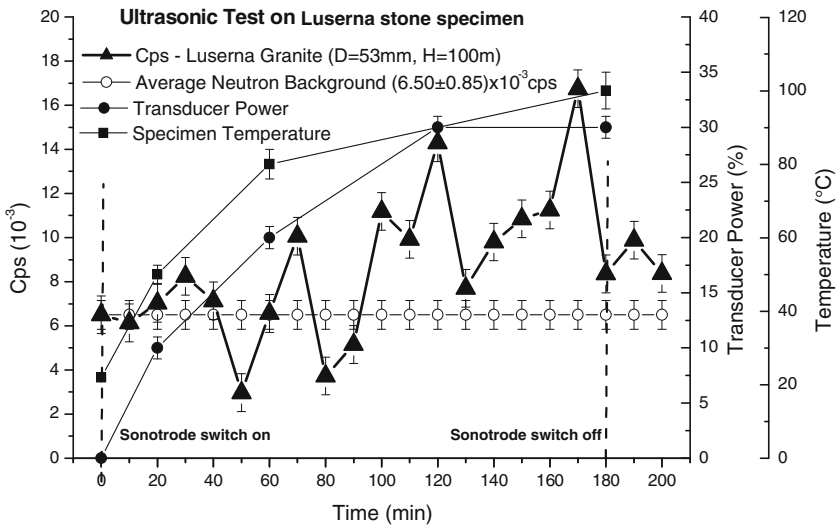

Fig. 8 Ultrasonic test. Neutron emissions compared with the specimen temperature and the transducer power trend

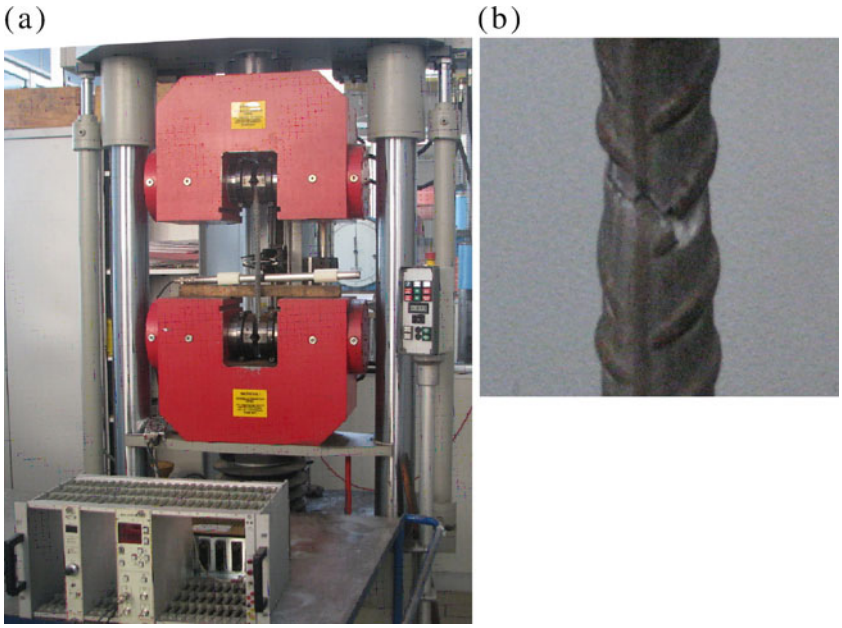

Fig. 10 (**a**) Experimental set-up for the tensile test performed on specimen S_1 using the Walter Bai hydraulic press. The He^3 neutron detector has been placed at a distance of about 10 cm from the monitored specimen. (**b**) Specimen S_1 at the end of the test [36]

loading ramp of 58 kN/min was applied and the test stopped after 34 min, at a load of 2,000 kN, corresponding to a specimen shortening approximately of 50 % (see Fig 11 (b)). Considering a symmetric behaviour of steel in tension and compression, the yield strength (638.56 kN) limit and the ultimate strength (850.31 kN) of specimen S_2 were identified considering the yielding stress and the ultimate strength obtained during the tensions test (see Table 4).

Neutron Emission Detections

Both the tension and compression tests performed on specimens S_1 and S_2 have been monitored by the He^3 neutron detector. In Figs. 10(a) and 11(a) the positions of the He^3 proportional counter are described together with the experimental set-up of the two tests.

In Fig. 12a, the load vs. time diagram for specimen S_1 is reported with the neutron emission measurements. The average neutron background level measured before the test was equal to $(7.22\pm1.42)\times10^{-2}$ cps. It can be noted that during the test, and in particular in correspondence to the achievement of the yield strength limit equal to 230 kN (see Fig 12(a)), neutron emissions increased up to $(11.67\pm2.29)\times10^{-2}$ cps. The increment $(4.45\pm2.69)\times10^{-2}$ cps was about 60 % of the background level. In addition, in correspondence to the ultimate strength (306 kN) a maximum neutron emission of about $(16.67\pm2.29)\times10^{-2}$ cps was measured. This last emission level corresponds to an increment close to 130 % with respect to the background level measured before the experiment. Finally, after the steel bar failure, the neutron emissions decreased almost instantaneously down to the background level measured before the experiment.

In Fig. 12(b), similarly to Fig. 12(a), the load versus time curve has been reported together with the neutron emission measurements for specimen S_2. Also in this case the neutron emissions show an appreciable increase immediately after the achievement of the ultimate strength (850 kN). At this point, the maximum neutron emission level $(19.99\pm2.96)\times10^{-2}$ cps) corresponds to an increment of about 170 % the background level. As can be seen from the diagram of Figs. 11(b) and 12(b), the final section area of specimen S_2 is sensibly larger than the initial nominal area, so that the theoretical ultimate strength was widely overcome.

Table 4 Tensile and compressive loading test on steel specimens

Tensile loading test: specimen S_1	
Section S_0	452.16 (mm^2)
Yield strength limit, P_y	230.00 (kN)
Ultimate strength, P_u	306.41 (kN)
Yielding stress, σ_y	508.66 (MPa)
Stress peak load, σ_u	677.65 (MPa)
Elongation at P_u, ε_u	38.18 (%)
Elongation at failure, ε_f	58.99 (%)
Compressive loading test: specimen S_2	
Section S_0	1256 (mm^2)
Yield strength limit, P_y	638.56 (kN)
Ultimate strength, P_u	850.31 (kN)

Compositional and Microchemical Evidence of Piezonuclear Fission Reactions in the Rock Specimens

Energy Dispersive X-ray Spectroscopy (EDS) was performed on different samples of external or fracture surfaces, belonging to the same specimens in Luserna stone used in

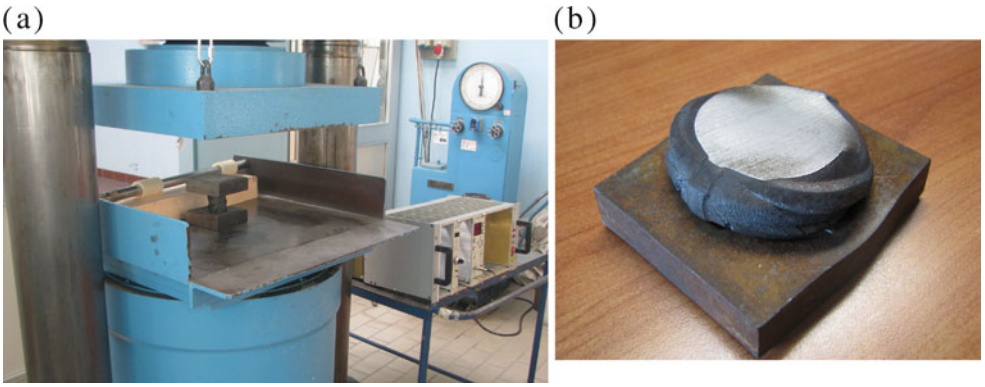

Fig. 11 (**a**) Experimental set-up for the compressive test performed on specimen S_2 using the Galdabini hydraulic press. The He^3 neutron detector has been placed at a distance of about 10 cm from the monitored specimen. (**b**) Specimen S_2 at the end of the test

the preliminary piezonuclear tests by Carpinteri et al. [1–3]. The tests were conducted in order to correlate the neutron emissions from the Luserna Granite with the variations in rock composition. These analyses lead to get averaged information of the mineral and chemical composition and to detect possible piezonuclear transmutations from iron to lighter elements. The quantitative elemental analyses were performed by a ZEISS Supra 40 Field Emission Scanning Electron Microscope (FESEM) equipped with an Oxford X-rays microanalyser. The samples were carefully chosen to investigate and compare the same crystalline phases both before and after the crushing failure. In particular, two crystalline phases, phengite and biotite, were considered due to their high iron content and relative abundances in the Luserna Granite (20 % and 2 %, respectively) [37].

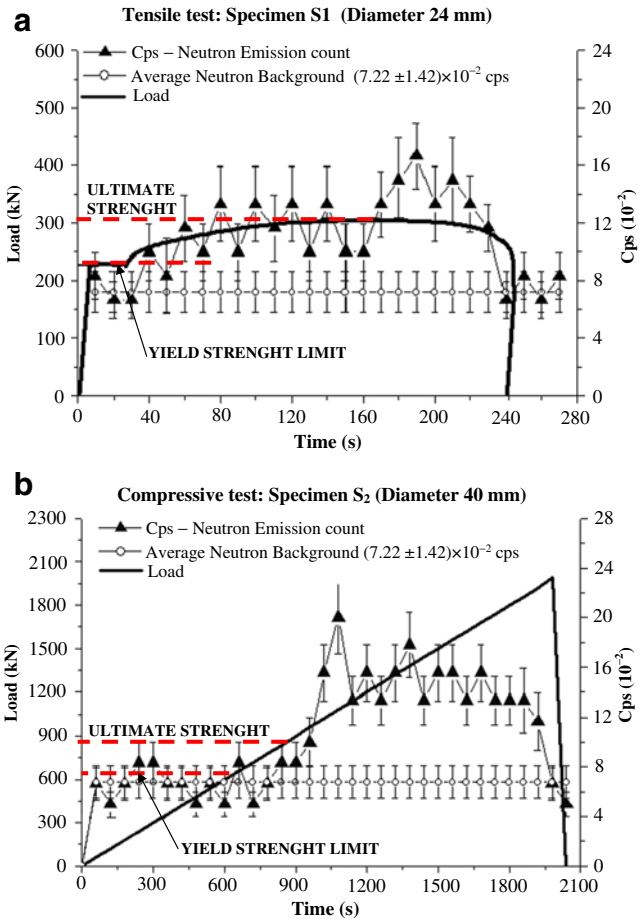

Fig. 12 Load vs. Time curves and neutron emission measurements for specimen S_1 (**a**) and S_2 (**b**). For specimen S_1 the maximum neutron emission level equal to $(16.67\pm2.29)\times10^{-2}$ cps, reached after the achievement of the ultimate strength, corresponds to an increment close to 130 % with respect to the background level. Similarly, for specimen S_2 it is possible to observe that the maximum neutron emission level, reached after the ultimate strength, equal to $(19.99\pm2.26)\times10^{-2}$ cps corresponds to an increment close to 170 % with respect to the same background level

Luserna "stone" is a leucogranitic orthogneiss, probably from the Lower Permian Age, that outcrops in the Luserna-Infernotto basin (Cottian Alps, Piedmont) at the border between the Turin and Cuneo provinces (North-western Italy) [38]. Characterized by a micro "Augen" texture, it is grey-greenish or locally pale blue in colour. Geologically, Luserna stone pertains to the Dora-Maira Massif [38, 39], that represents a part of the ancient European margin annexed to the Cottian Alps during Alpine orogenesis. From a petrographic point of view, it is the metamorphic result of a late-Ercinian leucogranitic rock transformation [37, 39]. The Luserna stone has a sub-horizontal attitude, with a marked fine-grained foliation that is mostly associated with visible lineation. The mineralogical composition includes K-feldspar (10–25 Wt. %), quartz (30–40 Wt. %), albite (15–25 Wt. %) and phengite (10–20 Wt. %); subordinated biotite, chlorite, zoisite and/or clinozoisite/epidote (less then 5 %). In addition to common accessory phases (ores, titanite, apatite and zircon), tourmaline, carbonates, rare axinite and frequent fluorite are present [37, 40].

In consequence of Luserna stone being a very heterogeneous rock, and in order to assess mass percentage variations in chemical elements such as Fe, Al, Si and Mg, the EDS analyses have been focused on two crystalline phases: phengite and biotite. These two minerals of granitic gneiss show a mineral chemistry in which the iron content is largely diffused (see Fig. 13(a) and (b)).

In Fig. 14(a), two thin sections obtained from the external surfaces of an integer and uncracked portion of one of the tested specimens are shown. The thin sections, finished with

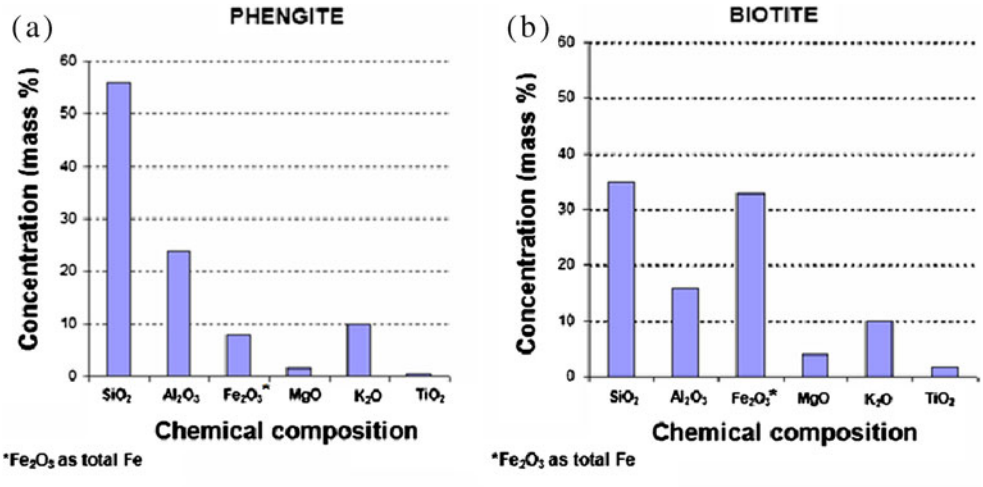

Fig. 13 (**a**) The chemical composition of phengite includes: SiO_2 (~56 %), Al_2O_3 (~24 %), Fe_2O_3 and FeO (~8 %) MgO (~1.5 %), Na_2O (~0.2 %) and K_2O (~10 %). (**b**) The chemical composition of biotite includes: SiO_2 (~35 %), Al_2O_3 (~16 %), Fe_2O_3 and FeO (~33 %), MgO (~3.5 %), TiO_2 (~1.5 %), and K_2O (~10 %)

a standard petrographic polishing procedure, present a rectangular geometry (45×27 mm) and are 30 μm thick. In Fig. 14(b), two portions of fracture surfaces taken from the same tested specimen are shown. For the EDS analyses, several phengite and biotite sites were localized on the surface of the thin sections and on the fracture surfaces. Sixty measurements of phengite crystalline phase, and thirty of biotite were selected and analysed. In Fig. 15(a) and (b), two electron microscope images of phengite and biotite sites, the first on the external sample (thin section 1) and the latter on the fracture surface (fracture surface 2), are shown.

EDS Results for Phengite

In Fig. 16(a) the results for the Fe concentrations obtained from the measurements on phengite crystalline phase are shown. Thirty of these measurements were carried out on the polished thin sections as representatives of the external surface samples, whereas the other thirty measurements were carried out on fracture surfaces. It can be observed that the distribution of Fe concentrations for the external surfaces, represented in the graph by squares, show an average value (calculated as the arithmetic mean value) equal to 6.20 %. In the same graph the distribution of Fe concentrations on the fracture samples (indicated by triangles) shows a significant variation. It can be seen that the mean value of the distribution of measurements performed on fracture surfaces is equal to 4.00 % and it is considerably lower than the mean value of external surface measurements (6.20 %). It is also interesting to note that the two Fe percentage distributions are separated by more than two standard deviations (σ=0.37 in the case of external surfaces and σ=0.52 in the case of fracture surfaces).

The iron decrease, considering the mean values of the distributions of phengite composition, is about 2.20 %. This iron content reduction corresponds to a relative decrease of 35 % with respect to the previous Fe content (6.20 % in phengite). Similarly to Fig. 16(a), the Al mass percentage concentrations are considered in both the cases of external and fracture surfaces. For Al contents, the percentage

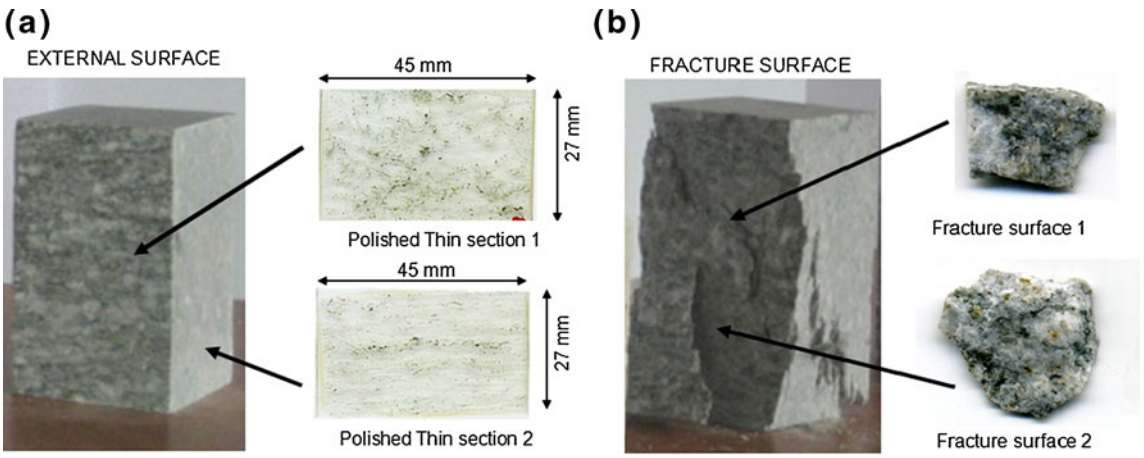

Fig. 14 (**a**) Polished thin sections obtained by the external surface of an integer and not fractured portion of the tested specimens [1, 3]. (**b**) Fracture surface belonging to the tested specimens [1–3]

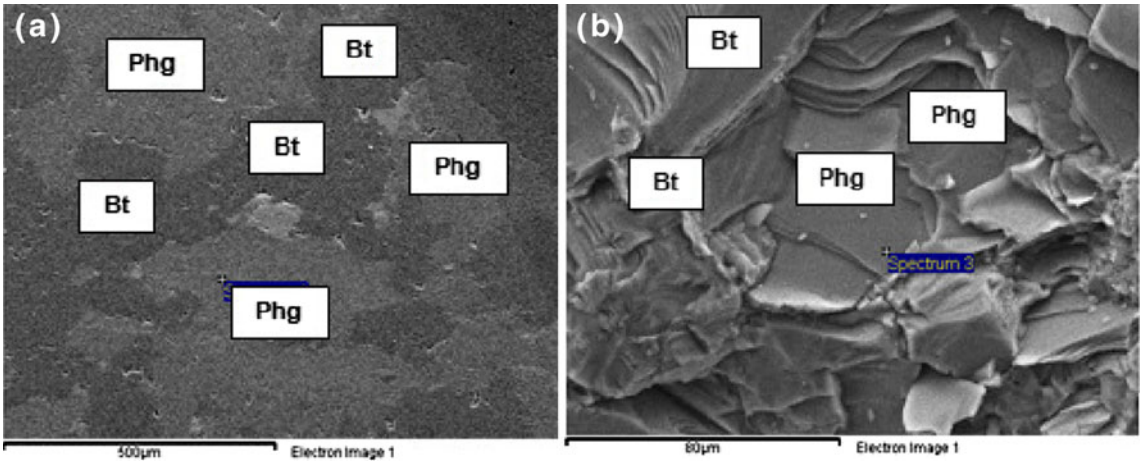

Fig. 15 FESEM images of phengite and biotite in the case of (**a**) external and (**b**) fracture sample

observed variations are approximately equal to that of Fe (compare Figs. 16(a) and 13(b)). The average increase in the distribution, corresponding to the fracture surfaces (indicated by triangles), is about 2.00 % of the phengite composition. The average value of Al concentrations changes from 12.50 % on the external surface to 14.50 % on the fracture surface. The relative increase in Al content is equal to 16 %.

The evidence emerging from the EDS analyses that the two values for the iron decrease (−2.20 %) and for the Al increase (+2.00 %) are approximately equal is really impressive. This fact is even more evident considering the trends of the other chemical elements constituting the mineral chemistry (excluding H and O) in phengite, because no appreciable variations can be recognized between the average values [24].

EDS Results for Biotite

In the Fig. 17(a)-(d) the results for Fe, Al, Si and Mg concentrations measured on 30 acquisition points of biotite crystalline phase are shown. These measurements were selected on the polished thin sections as representatives of the uncracked material samples (15 measurements) and on fracture surfaces (15 measurements). It can be observed that the distribution of Fe concentrations for the external surfaces, represented in Fig. 17(a) by squares, shows an average value (calculated as the arithmetic mean value) equal to 21.20 %. On the other hand, considering in the same graph the distribution of Fe concentrations on fracture samples (indicated by triangles), it can be seen that the mean value drops to 18.20 %. In this case, the iron decrease, considering the mean values of the Fe distributions, is about 3.00 %. This iron content reduction (−3.00 %) corresponds to a relative decrease of 14 % with respect to the previous Fe content (21.20 % in biotite). Similarly to Fig. 17(a), in Fig. 17(b) the Al mass percentage concentrations are considered in both cases of external and fracture samples. For Al contents the observed variations show an average increase of about 1.50 % in the biotite composition. The average value of Al

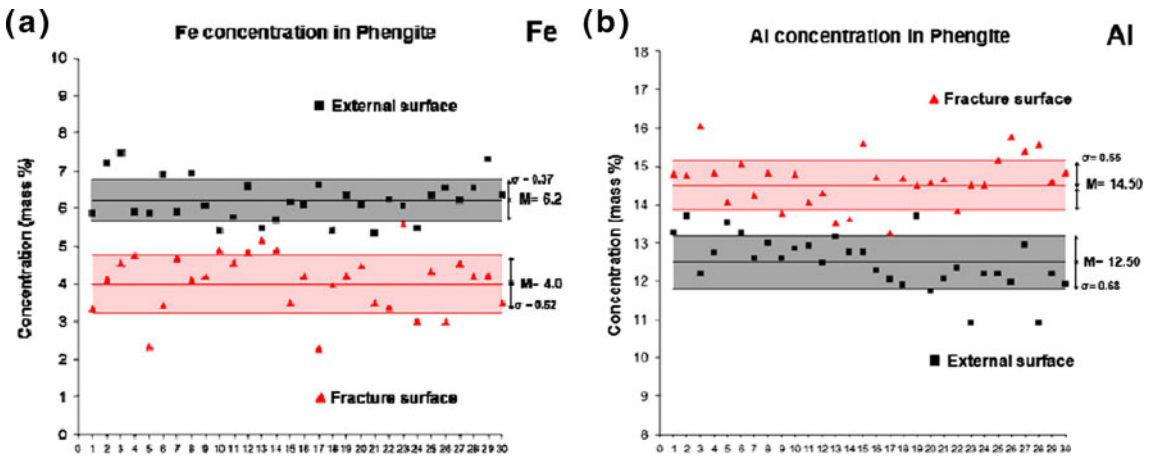

Fig. 16 Fe and Al concentrations in phengite: (**a**) Fe concentrations on external surfaces (*squares*) and on fracture surfaces (*triangles*). The Fe decrease considering the two mean values of the distributions is equal to 2.20 %. (**b**) Al concentrations on external surfaces (*squares*) and on fracture surfaces (*triangles*). The Al increase, considering the two mean values of the distributions, is equal to 2.0 %

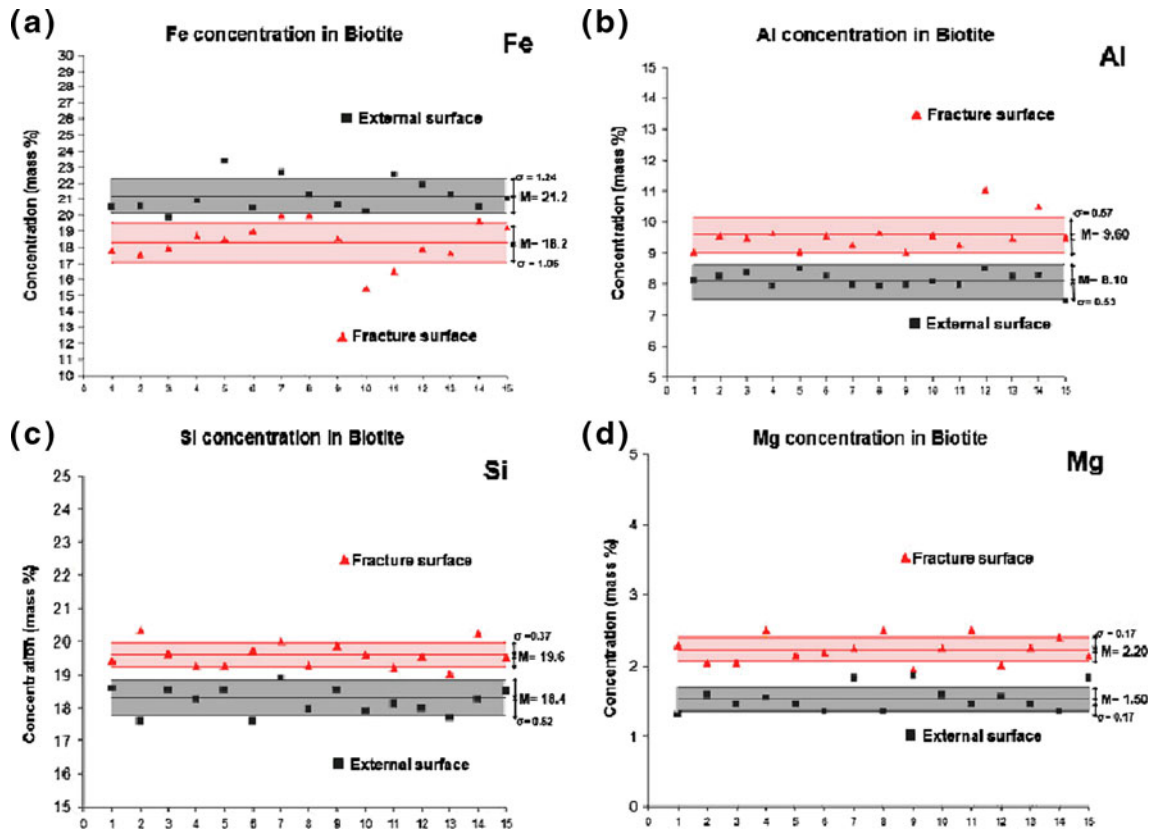

Fig. 17 Fe (**a**), Al (**b**), Si (**c**) and Mg (**d**) concentrations in biotite are reported for external and fracture surfaces. The iron decrease (−3.00 %) in biotite is counterbalanced by an increase in aluminum (+1.50 %), silicon (+1.20 %), and magnesium (+0.70 %). In the case of the other elements no appreciable variations can be recognized between the external and the fracture samples [24]

concentrations changes from 8.10 % on the external surface to 9.60 % on the fracture surface, with a relative increase in Al content equal to 18 %. In Fig. 17(c) and (d) it is shown that, in the case of biotite, also Si and Mg contents present considerable variations. Figure 17(c) shows that the mass percentage concentration of Si changes from a mean value of 18.40 % (external surface) to a mean value of 19.60 % (fracture surface) with an increase of 1.20 %. Similarly, in Fig. 17(d) the Mg concentration distributions show that the mean value of Mg content changes from 1.50 % (external surface) to 2.20 % (fracture surface). Therefore, the iron decrease (−3.00 %) in biotite is counterbalanced by an increase in aluminum (+1.50 %), silicon (+1.20 %), and magnesium (+0.70 %) [24].

Piezonuclear Reactions: From the Laboratory to the Planetary Scale

From the results shown in the previous sections and the experimental evidence reported in recent papers [1–3, 24], it can be clearly seen that piezonuclear reactions are possible in inert non-radioactive solids.

From the EDS results on fracture samples, the evidences of Fe and Al variations in phengite (Fig. 16) lead to the conclusion that the piezonuclear reaction:

$$\mathrm{Fe}_{26}^{56} \rightarrow 2\mathrm{Al}_{13}^{27} + 2\,\mathrm{neutrons} \quad (1)$$

should have occurred [1–3, 24]. Moreover, considering the evidences for the biotite content variations in Fe, Al, Si, and Mg (Fig. 17), it is possible to conjecture that another piezonuclear reaction, in addition to (1), should have occurred during the piezonuclear tests [1–3, 24]:

$$\mathrm{Fe}_{26}^{56} \rightarrow \mathrm{Mg}_{12}^{24} + \mathrm{Si}_{14}^{28} + 4\,\mathrm{neutrons} \quad (2)$$

Taking into account that granite is a common and widely occurring type of intrusive, sialic, igneous rock, and that it is characterized by an extensive concentration in the rocks that make up the Earth's crust (~60 % of the Earth's crust), the piezonuclear fission reactions expressed above can be generalized from the laboratory to the Earth's crust scale, where mechanical phenomena of brittle fracture, due to fault collision and subduction, take place continuously in the most seismic areas. This hypothesis seems to find surprising evidence and confirmation from both the geomechanical and the geochemical points of view [25]. The neutron

emissions involved in piezonuclear reactions can be detected not only in the laboratory experiments, as shown in [1–3], but also at the Earth's crust scale. Recent neutron emission detections have led to consider also the Earth's crust, in addition to cosmic rays, as a relevant source of neutron flux variations [41, 42]. Neutron emissions measured at seismic areas in the Pamir region (4,200 m asl) exceeded the usual neutron background up to three orders of magnitude in correspondence to seismic activity and rather appreciable earthquakes, greater than or equal to the 4th degree in the Richter scale magnitude [43].

This relationship between the processes in the Earth's crust and neutron flux variations has allowed methods for short-term prediction and monitoring of earthquakes to be developed [41, 42]. Neutron flux variations, in correspondence to seismic activity, may be evidence of changes in the chemical composition of the crust, as a result of piezonuclear reactions.

The present natural abundances of aluminum (~8 %), silicon (~28 %) and magnesium (~1.3 %) and scarcity of iron (~4 %) in the continental Earth's crust [27, 44, 45] are possibly due to the piezonuclear fission reactions (1,2) expressed above [25]. In addition, considering the mass percentage concentrations of other chemical elements, such as Na (~2.9 %), Ni (~0.01 %), and Co (0.003 %), in the continental crust [26, 27, 44–48], it is possible to conjecture additional piezonuclear fission reactions that could have taken place in correspondence to plate collision and subduction [25]:

$$\mathrm{Co}_{27}^{59} + \mathrm{Al}_{13}^{27} + \mathrm{Si}_{14}^{28} + 4\,\mathrm{neutrons} \tag{3}$$

$$\mathrm{Ni}_{28}^{59} \rightarrow 2\,\mathrm{Si}_{14}^{28} + 3\,\mathrm{neutrons} \tag{4}$$

$$\mathrm{Ni}_{28}^{59} \rightarrow \mathrm{Na}_{11}^{23} + \mathrm{Cl}_{17}^{35} + 1\,\mathrm{neutron} \tag{5}$$

The large concentrations of granite minerals, such as quartz and feldspar (SiO_2, Al_2O_3) in the Earth's crust, and to a lesser extent of magnesite, halite, and zeolite (MgO, Na_2O, Cl_2O_3), and the low concentrations of magnetite, hematite, bunsenite and cobaltite (composed predominantly of Fe, Co, and Ni minerals), could be ascribed to piezonuclear reactions (1–5) produced by tectonic and subduction phenomena [25].

Heterogeneity in the Composition of the Earth's Crust: Fe and Al Reservoir Localizations

The localization of Al and Fe mineral reservoirs seems to be closely connected to the geological periods when different continental zones were formed [27, 49–53]. This fact would seem to suggest that our planet has undergone a continuous evolution from the most ancient geological regions, which currently reflect the continental cores that are rich in Fe reservoirs, to more recent or contemporary areas of the Earth's crust where the concentrations of Si and Al oxides present very high mass percentages [27, 50, 51]. The main iron reservoir locations (Magnetite and Hematite mines) are reported in Fig. 18(a) [49–53]. The main concentrations of Al-oxides and rocky andesitic formations (the Rocky Mountains and the Andes, with a strong concentration of Al_2O_3 minerals) are shown in Fig. 18(b) together with the most important subduction lines, tectonic plate trenches and rifts [27, 50, 51]. The geographical locations of the main bauxite mines show that the largest concentrations of Al reservoirs can be found in correspondence to the most seismic areas of the Earth (Fig. 18(b)). The main iron mines are instead exclusively located in the oldest and interior parts of continents (formed through the eruptive activity of the proto-Earth), in geographic areas with a reduced seismic risk and always far from the main fault lines. From this point of view, the close correlation between bauxite and andesitic reservoirs and the subduction and most seismic areas of the Earth's crust provides a very impressive evidence of piezonuclear effects at the planetary scale.

Geochemical Evidence of Piezonuclear Reactions in the Evolution of the Earth's Crust Chemical Elements

Evidence of piezonuclear reactions can be also recognized considering the Earth's composition and its way of evolving throughout the geologic eras. In this way, plate tectonics and the connected plate collision and subduction phenomena are useful to understand not only the morphology of our planet, but also its compositional evolution [25].

From 4.0 to 2.0 Gyrs ago, Fe could be considered one of the most common bio-essential elements required for the metabolic action of all living organisms [54–62]. Today, the deficiency of this nutrient suggests it as a limiting factor for the development of marine phytoplankton and life on Earth [26, 56]. Elements such as Fe and Ni in the Earth's protocrust had higher concentrations in the Hadean (4.5–3.8 Gyr ago) and Archean (3.8–2.5 Gyr ago) periods compared to the present values [44, 45, 56, 57, 63–68]. The Si and Al concentrations instead were lower than they are today [27, 44, 45, 63–66].

The estimated concentrations of Fe, Ni, Al, and Si in the Hadean and Archean Earth's protocrust and in the present Earth's continental crust are reported in Fig. 19. The data for the Hadean period (4.5–3.8 Gyrs ago) are referred to the composition of Earth's protocrust, considering the assumptions made by Foing [59] and by Taylor and Mclennan [44,

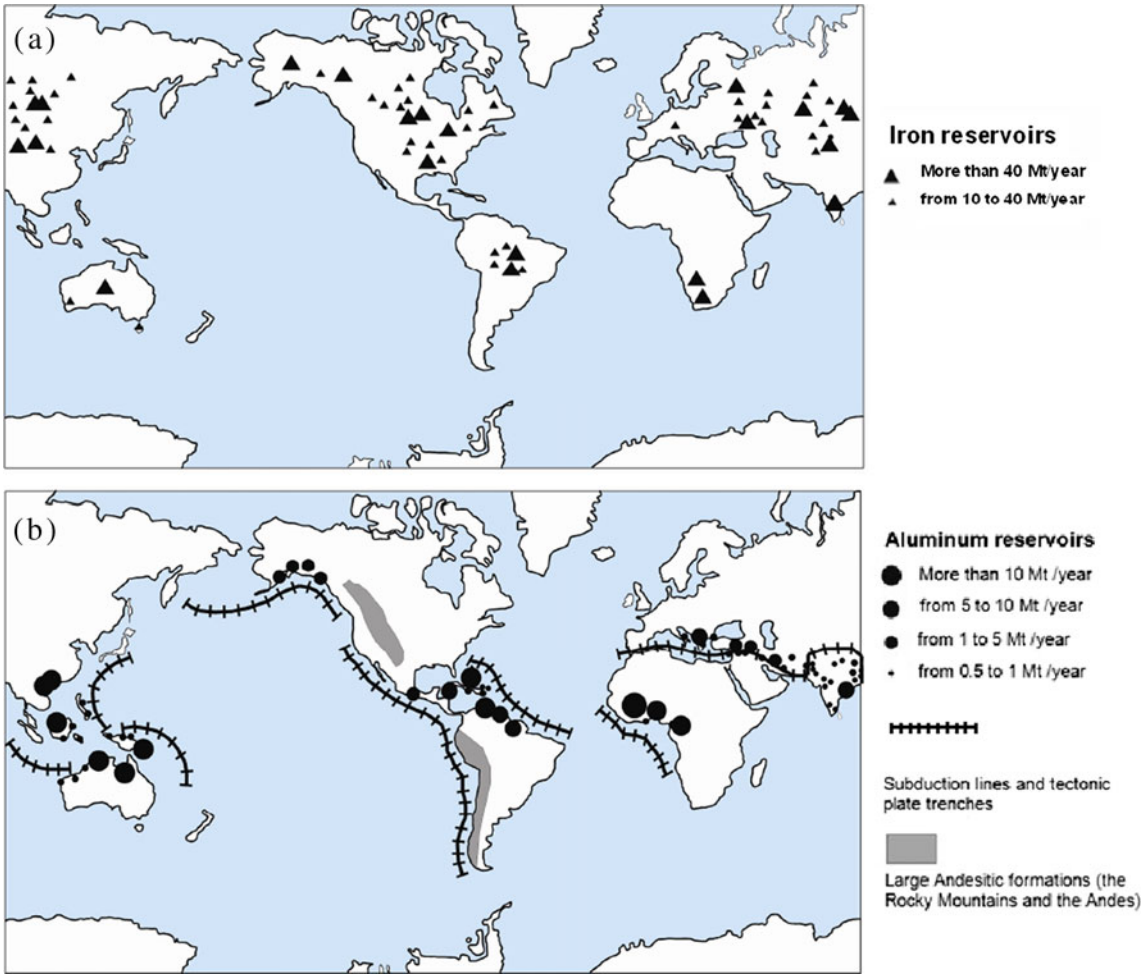

Fig. 18 (**a**) Locations of the largest iron mines in the world [49–51]. Iron ore reservoirs (Magnetite and Hematite mines) are located in geographic areas with reduced seismic risks and always far from fault lines. (**b**) The largest aluminum (bauxite) reservoirs are reported together with the main Andesitic formations and most important subduction lines and plate tectonic trenches [27]

45]. According to these authors, the Mars and Moon's crusts are considered to be representative of the composition of the early Earth's protocrust (Hadean Eon) that was strongly basaltic, with a composition similar to that of the proto-planets (chondrites) [44, 45, 55, 59]. In the same Figure, for the Archean period (3.8–2.5 Gyrs ago) the data are referred to compositional analysis of Archean sediments [25, 27, 44, 45, 48, 67–69]. For the last period from 2.5 Gyrs ago to today, the mass percentage concentrations of Fe, Ni, Al and Si are referred to the present composition of Earth's continental crust [25, 27, 44, 45, 70, 71].

A clear transition from a more basaltic condition (high concentrations of Fe and Ni) to a sialic one (high concentrations of Si and Al) can be observed during the life time of our planet [27, 44, 45, 47, 48, 60–71].

The most abrupt changes in element concentrations shown in Fig. 19 appear to be intimately connected to the tectonic activity of the Earth. The vertical drops in the concentrations of Fe and Ni, as well as the vertical jumps in the concentrations of Si and Al, 3.8 Gyrs ago, coincide with the time that many scientists have pointed out as the beginning of tectonic activity on the Earth. The subsequent abrupt transitions 2.5 Gyrs ago coincide with the period of the Earth's largest and most intense tectonic activity [44, 45].

From the data reported in Fig. 19, a decrease of ~7 % in Fe and ~0.2 % in Ni concentrations can be observed between the Hadean period (4.5–3.8 Gyrs ago) and the Archean period (3.8–2.5 Gyrs ago) [27, 44, 45, 47, 67–70]. At the same time, Al and Si concentrations increase of ~3 % and ~2 % respectively. Similarly, a global decrease of ~5 % in the concentrations of Fe (~4 %) and Ni (~1 %) and a global increase of about 3 % in the concentrations of Si (~2 %) and Al (~1 %) are shown between the Archean period (3.8–2.5 Billion years ago) and more recent times (Fig. 19). The balances between heavier (Fe and Ni) and lighter elements (Si and Al) could be considered as perfectly satisfied taking into account a virtual increase in Mg similar to that of Si over

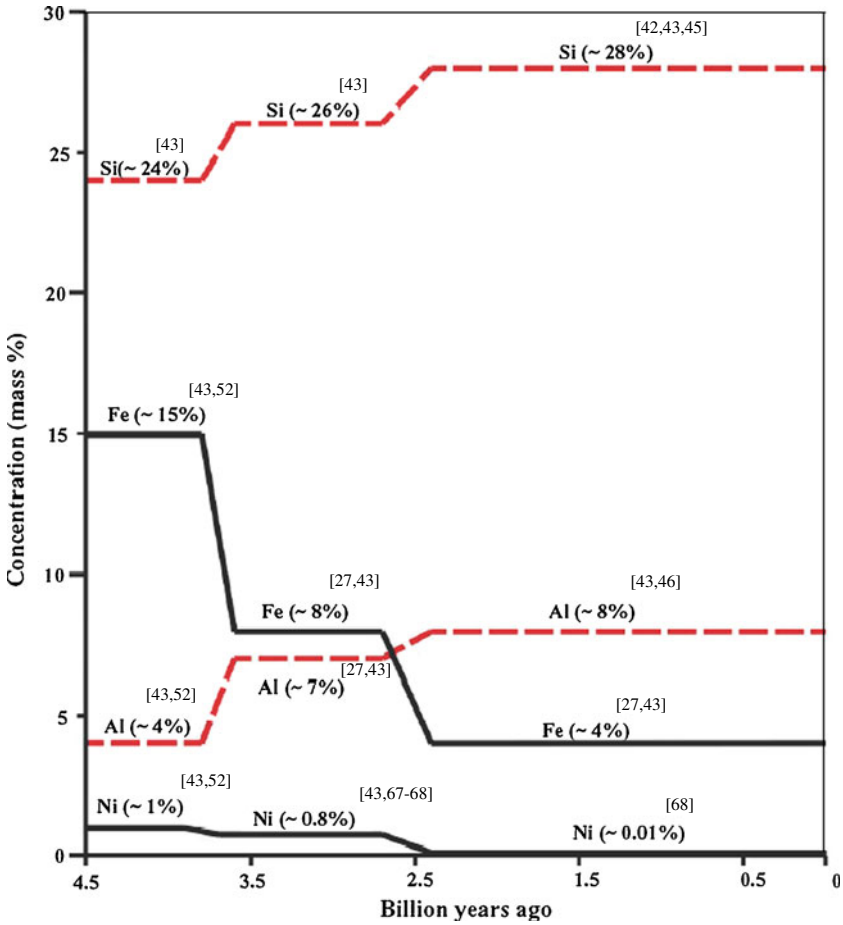

Fig. 19 The estimated concentrations of Fe, Ni, Al, and Si in the Hadean and Archean Earth's protocrust and in the Earth's continental crust are reported. The Archean Earth's protocrust (3.8–2.5 Gyrs ago) had a less basaltic composition (Fe ~8 %, Ni ~0.8 %, Al ~7 %, Si ~26 %) [27, 42, 45, 47, 67–69] compared to the previous period (Hadean Era, 4.5–3.8 Gyrs ago) [43, 52], and a less Sialic composition compared to the concentrations in the Earth's continental crust today: Fe ~4 %, Ni ~0.01 %, Al ~8 %, Si ~28 %. [27, 44, 45, 67–70]. Considering piezonuclear reactions (1,2,4), the overall 12 % decrease in the heavier elements (Fe and Ni) is balanced by the Al and Si increases and assuming an increase in Mg, according to reaction (2), equal to that of Si over the last 4.5 Billion years

the Earth's lifetime. This Mg increase cannot be deduced from the geological data of ancient sediments.

The most probable explanation is that Mg is not only a resulting element, as shown by piezonuclear reaction (2), but can also be considered as a starting element of other possible piezonuclear reactions [25], like for example:

$$Mg_{12}^{24} \rightarrow 2C_{6}^{12}. \quad (6)$$

Reaction (6) could be very important for the evolution of both the Earth's crust and atmosphere, and considered as a valid explanation for the high level of CO_2 concentration (~15 %) in the Archean Earth's atmosphere [72]. In addition, the large amount of C produced by Mg transformation (~4.0 % of the Earth's crust) has undergone a slow but continuous diminishing in the CO_2 composition of the Earth's atmosphere, as a result of the escape which also involves other atmospheric gases liken, O, He and H [73].

Piezonuclear reaction (6) can also be put into correlation with the increase in seismic activity that has occurred over the last century [74]. Very recent evidence has shown CO_2 emissions in correspondence to seismic activity [75]: significant increase in the emission of carbon dioxide was recorded in a geochemical station at El Hierro, in the Canary Islands, before the occurrence of several seismic events during the year 2004. Appreciable precursory CO_2 emissions were observed to start before seismic events of relevant magnitude, and to reach their maximum values some days before the earthquakes [75].

Relation (6) is not the only piezonuclear reaction that involves Mg as a starting element. Like the considerations made for the concentrations of elements such as Fe, Ni, Al, and Si (Fig. 19), it is also possible to consider other elements such as Mg, Ca, Na, K, and O, which are involved in other piezonuclear reactions that have been assumed to occur in the chemical evolution of the Earth's crust [25].

The variations in mass percentage for Mg, Ca, Na, K, and O in the Hadean and Archean Earth's protocrust and in the present Earth's continental crust are reported in Fig. 20, analogously to Fig. 19 [25, 27, 44, 45, 71].

The decrease in the mass concentrations of Mg and Ca has been balanced by an increase in Na, K, and O, during the Earth's lifetime [27, 44, 45, 71]. In particular, between the Hadean (4.5–3.8 Gyr ago) and the Archean era (3.8–2.5 Gyrs ago), and between the latter and more recent times, it is possible to observe an overall decrease of ~4.7 % in Mg and ~4.0 % in Ca. This decrease in the two alkaline-earth metals (Mg and Ca) seems to be nearly perfectly

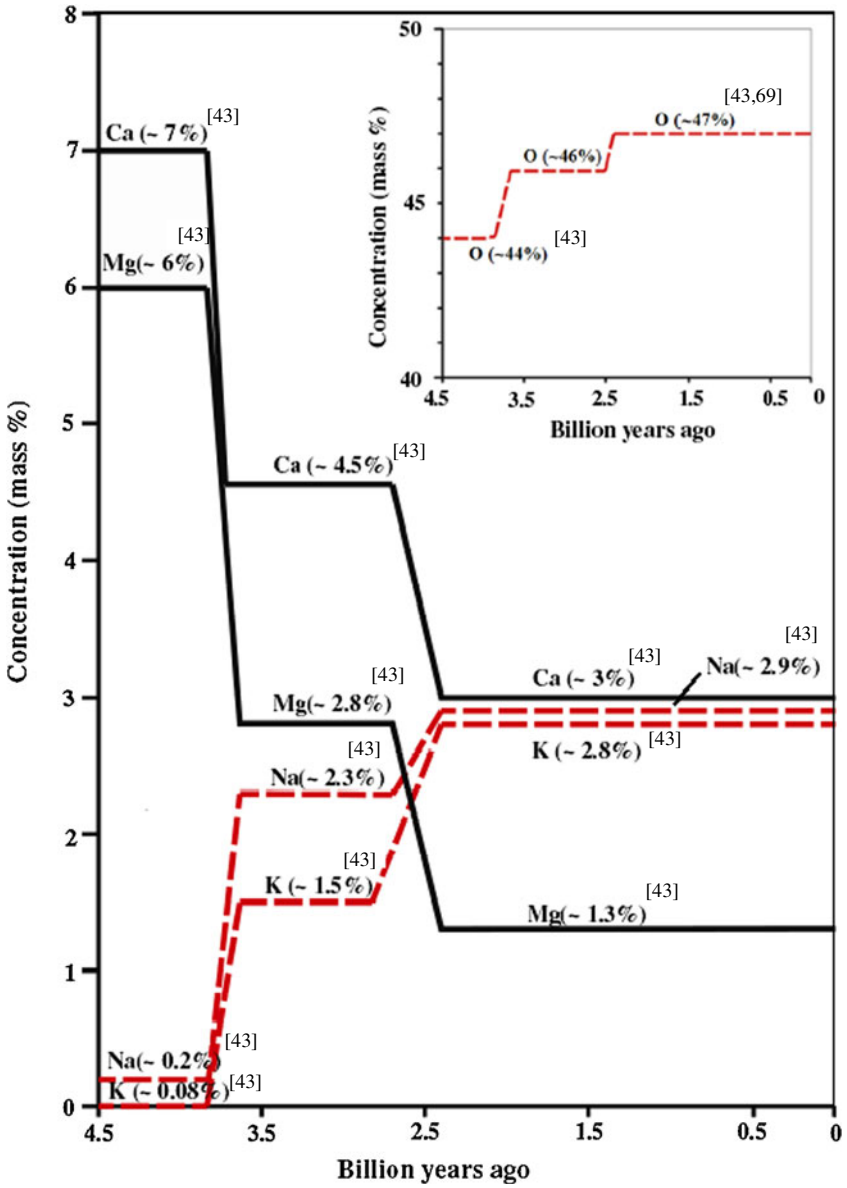

Fig. 20 The variations in mass percentage concentration for Mg, Ca, Na, K, and O in the Hadean and Archean Earth's protocrust and in the Earth's continental crust are reported. It can be noted in particular that, considering piezonuclear reactions (7–10), the overall 8.7 % decrease in alkaline-earth metals (Mg and Ca) is balanced by the Na, K, and O increase (~8.5 %) [27, 44, 45, 71]

balanced by the increase in the concentrations of the two alkaline metals, Na and K (which have increased by 2.7 % and 2.8 %, respectively), and by a total increase of ~3 % in O, which has varied from ~44 % to ~47 % (the latter being the present Oxygen concentration in the Earth's Crust) (Fig. 20). Also in this case, the greatest changes in the Earth's Crust are strictly connected with the most intense seismic activity in the planet. From a close examination of the data reported in Fig. 20, it is possible to conjecture a series of piezonuclear fission reactions that could represent the real origin of the sharp fluctuations of these chemical elements in the evolution of the Earth's crust:

$$\mathrm{Mg}_{12}^{24} \rightarrow \mathrm{Na}_{11}^{23} + \mathrm{H}_{1}^{1} \tag{7}$$

$$\mathrm{Mg}_{12}^{24} \rightarrow \mathrm{O}_{8}^{16} + 4\mathrm{H}_{1}^{1} + 4\,\mathrm{neutrons} \tag{8}$$

$$\mathrm{Ca}_{20}^{40} \rightarrow \mathrm{K}_{19}^{39} + \mathrm{H}_{1}^{1} \tag{9}$$

$$\mathrm{Ca}_{20}^{40} \rightarrow 2\mathrm{O}_{8}^{16} + 4\mathrm{H}_{1}^{1} + 4\,\mathrm{neutrons} \tag{10}$$

In particular, The overall 12 % decrease in the heavier elements (Fe and Ni) reported in Fig. 19 could be perfectly balanced by the Al, Si and Mg increase (~12 %) over the last 4.5 Billion years. At 3.8 Billions years ago, in fact, we can consider the following balance: Fe (−7 %)+Ni (−0.2 %)=Al (+3 %)+Si (+2.4 %)+Mg (+1.8 %). Analogously at 2.5 Billions years ago we have: Fe (−4 %)+Ni (−0.8 %)=Al (+1 %)+Si (+2.4 %)+Mg (+1.4 %). The increases in Si and Mg are not perfectly the same due to the fact that Si is involved at the same time in reactions (2) and (4) and for the different mass number of the two elements. Analogously, considering piezonuclear reactions (7–10), an overall decrease in alkaline-earth metals (Mg and Ca) of about 8.7 % is

balanced by an increase in Na, K, and O (see Fig. 20). At 3.8 Billions years ago, we have the following balance (see Fig. 20): Ca (−2.5 %)+Mg(−3.2 %)=K (+1.4 %)+Na (+2.1 %)+O (+2.2 %). At 2.5 Billions years ago, on the other hand we have: Ca (−1.5 %)+Mg(−1.5 %)=K (+1.3 %)+Na (+0.6 %)+O (+1.1 %).

Conclusions

Neutron emission measurements were performed on Luserna stone specimens during mechanical tests. From these experiments, it can be clearly seen that piezonuclear reactions giving rise to neutron emissions are possible in inert non-radioactive solids under pressure loading. In particular, during compression tests of specimens of sufficiently large size, the neutron flux was found to be of about one order of magnitude higher than the background level at the time of catastrophic failure. For test specimens with more ductile behaviour, neutron emissions significantly higher than the background were also found. Neutron detection is also confirmed in compression test under cyclic loading and during ultrasonic vibration. In addition, neutron emission measurements were conducted on steel specimens under tension and compression loading, finding an increase of 130 % with respect to the background neutron level in correspondence to the ultimate strength.

Our conjecture, also confirmed by the Energy Dispersive X-ray Spectroscopy (EDS) tests, is that piezonuclear reactions, produced without gamma emission, involving fission of iron into aluminum, or into magnesium and silicon, should have occurred during compression on the tested specimens. Nuclear structure physics is not a closed question and the recent evidence of piezonuclear fission reactions from earthquakes and brittle rocks failure [1–5, 24, 25, 42–44] find necessary to re-open this field to address old problems or to explain new phenomena such as these new kinds of low energy nuclear reactions [76, 77]. Even small deviations from classical assumptions, e.g., from the concept of average binding energy per nucleon, could explain these new phenomena. It would suffice to assume a weak section within the nucleus, as it analogously happens in very hard and strong rocks that nevertheless cleave under very low stresses.

Finally, the hypothesis of piezonuclear reactions seems to find surprising evidence and confirmation at the Earth crust scale from both geomechanical and geochemical points of view. The piezonuclear reactions have thus been considered in order to interpret the most significant geophysical and geological transformations, today still unexplained.

Acknowledgments The financial support provided by the Regione Piemonte (Italy) RE-FRESCOS Project, is gratefully acknowledged.

Special thanks are due to R. Sandrone and A. Chiodoni from the Politecnico di Torino for their kind collaboration in the EDS analysis. The authors wish to thank also D. Madonna Ripa and A. Troia from the National Research Institute of Metrology – INRIM, for their valuable assistance during the ultrasonic tests.

References

1. Carpinteri A, Cardone F, Lacidogna G (2009) Piezonuclear neutrons from brittle fracture: early results of mechanical compression tests. Strain 45:332–339
2. Cardone F, Carpinteri A, Lacidogna G (2009) Piezonuclear neutrons from fracturing of inert solids. Phys Lett A 373:4158–4163
3. Carpinteri A, Cardone F, Lacidogna G (2010) Energy emissions from failure phenomena: mechanical, electromagnetic, nuclear. Exp Mech 50:1235–1243
4. Carpinteri A, Borla O, Lacidogna G, Manuello A (2010) Neutron emissions in brittle rocks during compression tests: monotonic vs cyclic loading. Phys Mesomech 13:268–274
5. Carpinteri A, Lacidogna G, Manuello A, Borla O (2011) Energy emissions from brittle fracture: neutron measurements and geological evidences of piezonuclear reactions. Strenght Fract Complex 7:13–31
6. Mogi K (1962) Study of elastic shocks caused by the fracture of heterogeneous materials and its relation to earthquake phenomena. Bull Earthq Res Inst 40:125–173
7. Lockner DA, Byerlee JD, Kuksenko V, Ponomarev A, Sidorin A (1991) Quasi static fault growth and shear fracture energy in granite. Nature 350:39–42
8. Shcherbakov R, Turcotte DL (2003) Damage and self-similarity in fracture. Theor Appl Fract Mech 39:245–258
9. Ohtsu M (1996) The history and development of acoustic emission in concrete engineering. Mag Concr Res 48:321–330
10. Carpinteri A, Lacidogna G, Pugno N (2006) Richter's laws at the laboratory scale interpreted by acoustic emission. Mag Concr Res 58:619–625
11. Carpinteri A, Lacidogna G, Niccolini G (2006) Critical behaviour in concrete structures and damage localization by acoustic emission. Key Eng Mater 312:305–310
12. Carpinteri A, Lacidogna G, Pugno N (2007) Structural damage diagnosis and life-time assessment by acoustic emission monitoring. Eng Fract Mech 74:273–289
13. Carpinteri A, Lacidogna G, Niccolini G (2009) Fractal analysis of damage detected in concrete structural elements under loading. Chaos Solitons Fractals 42:2047–2056
14. Carpinteri A, Lacidogna G, Puzzi S (2009) From criticality to final collapse: evolution of the b-value from 1.5 to 1.0. Chaos Solitons Fractals 41:843–853
15. Carpinteri A, Lacidogna G, Niccolini G, Puzzi S (2009) Morphological fractal dimension versus power-law exponent in the scaling of damaged media. Int J Damage Mech 18:259–282
16. Miroshnichenko M, Kuksenko V (1980) Study of electromagnetic pulses in initiation of cracks in solid dielectrics. Sov Phys-Solid State 22:895–896
17. Warwick JW, Stoker C, Meyer TR (1982) Radio emission associated with rock fracture: possible application to the great Chilean earthquake of May 22, 1960. J Geophys Res 87:2851–2859
18. O'Keefe SG, Thiel DV (1995) A mechanism for the production of electromagnetic radiation during fracture of brittle materials. Phys Earth Planet Inter 89:127–135
19. Scott DF, Williams TJ, Knoll SJ (2004) Investigation of electromagnetic emissions in a deep underground mine. Proc. of the 23rd

Int. Conf. on Ground Control in Mining, Morgantown, 3-5 August 2004, 125–132
20. Frid V, Rabinovitch A, Bahat D (2003) Fracture induced electromagnetic radiation. J Phys D 36:1620–1628
21. Rabinovitch A, Frid V, Bahat D (2007) Surface oscillations. A possible source of fracture induced electromagnetic oscillations. Tectonophysics 431:15–21
22. Lacidogna G, Carpinteri A, Manuello A, Durin G, Schiavi A, Niccolini G, Agosto A (2011) Acoustic and electromagnetic emissions as precursor phenomena in failure processes. Strain 47(suppl 2):144–152
23. Carpinteri A, Lacidogna G, Manuello A, Niccolini A, Schiavi A, Agosto A (2010) Mechanical and electromagnetic emissions related to stress-induced cracks. Exp Tech. doi:10.1111/j.1747-1567.2011.00709.x
24. Carpinteri A, Chiodoni A, Manuello A, Sandrone R (2011) Compositional and microchemical evidence of piezonuclear fission reactions in rock specimens subjected to compression tests. Strain 47(suppl 2):282–292
25. Carpinteri A, Manuello A (2011) Geomechanical and geochemical evidence of piezonuclear fission reactions in the Earth's crust. Strain 47(suppl 2):267–281
26. Anbar AD (2008) Elements and evolution. Science 322:1481–1482
27. Favero G, Jobstraibizer P (1996) The distribution of aluminum in the Earth: from cosmogenesis to Sial evolution. Coord Chem Rev 149:467–400
28. Konhauser KO, Pecoits E, Lalonde SV, Papineau D, Nisbet EG, Barley ME, Arndt NT, Zahnle K, Kamber BS (2009) Oceanic nickel depletion and a methanogen famine before the great oxidation event. Nature 458:750–754
29. Lacidogna G, Manuello A, Carpinteri A, Niccolini G, Agosto A, Durin G (2010) Acoustic and electromagnetic emissions in rocks under compression. Proc. of SEM Annual Conf. & Expo. on Exp. and Appl. Mechanics, Indianapolis, 7–10 June 2010, Paper N. 433
30. Bubble Technology Industries (1992) Instruction manual for the bubble detector. Chalk River, Ontario, Canada
31. National Council on Radiation Protection and Measurements (1971) Protection against neutron radiation, NCRP Report 38
32. Carpinteri A (1989) Cusp catastrophe interpretation of fracture instability. J Mech Phys Solids 37:567–582
33. Carpinteri A (1990) A catastrophe theory approach to fracture mechanics. Int J Fract 44:57–69
34. Cardone F, Cherubini G, Petrucci A (2009) Piezonuclear neutrons. Phys Lett A 373:862–866
35. Cardone F, Mignani R, Petrucci A (2009) Piezonuclear decay of thorium. Phys Lett A 373:1956–1958
36. EN ISO 6892 – 1:2009 (2009) Metallic materials – tensile testing – part 1: method of test at room temperature
37. Vola G, Marchi M (2009) Mineralogical and petrographic quantitative analysis of a recycled aggregate from quarry wastes. The Luserna stone case-study. Proc. of the 12th Euroseminar on Microscopy Appl. to Building Mat., 15–19 September 2009, Dortmund, Germany (2009)
38. Sandrone R, Cadoppi P, Sacchi R, Vialon P (1993) The Dora-Maira massif. In: Von Raumer JF, Neubauer F (eds) Pre-mesozoic geology in the Alps. Springer, Berlin, pp 317–325
39. Compagnoni R, Crisci GM, Sandrone R (1983) Caratterizzazione chimica e petrografica degli"gneiss di Luserna" (Massiccio cristallino Dora-Maira, Alpi Occidentali). Rend Soc It Min Petr 38:498
40. Sandrone R, Colombo A, Fiora L, Fornaro M, Lovera E, Tunesi A, Cavallo A (2004) Contemporary natural stones from the Italian western Alps (Piedmont and Aosta Valley regions). Periodico di Mineralogia (Special issue) 73:211–226
41. Kuzhevskij M, Nechaev OYu, Sigaeva EA, Zakharov VA (2003) Neutron flux variations near the Earth's crust. A possible tectonic activity detection. Nat Hazards Earth Syst Sci 3:637–645
42. Kuzhevskij M, Nechaev OYu, Sigaeva EA (2003) Distribution of neutrons near the Earth's surface. Nat Hazard Earth Syst Sci 3:255–262
43. Volodichev NN, Kuzhevskij BM, Yu NO, Panasyuk MI, Podorolsky AN, Shavrin PI (2000) Sun-Moon-Earth connections: the neutron intensity splashes and seismic activity. Astron Vestn 34:188–190
44. Taylor SR, McLennan SM (1995) The geochemical evolution of the continental crust. Rev Geophys 33:241–265
45. Taylor SR, McLennan SM (2009) Planetary crusts: their composition, origin and evolution. Cambridge University Press, Cambridge
46. Fowler CMR (2005) The solid earth: an introduction to global geophysics. Cambridge University Press, Cambridge
47. Doglioni C (2007) Interno della Terra. Treccani, Enciclopedia Scienza e Tecnica 595–605
48. Rudnick RL, Fountain DM (1995) Nature and composition of the continental crust: a lower crustal perspective. Rev Geophys 33:267–309
49. Roy I, Sarkar BC, Chattopadhyay A (2001) MINFO-a prototype mineral information database for iron ore resourcers of India. Comp Geosci 27:357–361
50. World Iron Ore producers. Available at http://www.mapsofworld.com/minerals/world-iron-ore-producers.html; last accessed October 2009
51. World Mineral Resources Map. Available at http://www.mapsofworld.com/world-mineral-map.htm; last accessed October 2009
52. Key Iron Deposits of the World. Available at http://www.portergeo.com.au/tours/iron2002/-iron2002depm2b.asp; last accessed October 2009
53. Lunine JIE (1998) Earth: evolution of a habitable world. Cambridge University Press, Cambridge, New York, Melbourne
54. Hazen RM et al (2008) Mineral evolution. Am Mineral 93:1693–1720
55. Condie KC (1976) Plate Tectonics and crustal evolution. Pergamon Press, Elmsford
56. Canfiled DE (1998) A new model for Proterozoic ocean chemistry. Nature 396:450–453
57. Holland HD (2006) The oxygenation of the atmosphere and oceans. Philos Trans R Soc London Ser B 361:903–915
58. Kholodov VN, Butuzova GY (2008) Siderite formation and evolution on sedimentary iron ore deposition in the Earth's history. Geol Ore Depos 50:299–319
59. Foing B (2005) Earth's childhood attic. *Astrobiol. Mag.* Retrospection (on-line) February 23 2005: http://www.astrobio.net/news/article1456.html
60. Sigman D et al (2004) Polar ocean stratification in a cold climate. Nature 428:59–63
61. Galimov EM (2005) Redox evolution of the Earth caused by a multistage formation of its core. Earth Plan Sci Lett 233:263–276
62. Yamaguchi KE (2005) Evolution of the geochemical cycle of Fe trough geological time: iron isotope perspective. Front Res Earth E 2:4–24
63. Basile-Doelsch I (2006) Si stable isotope in the Earth's surface: a review. J Geochem Explor 88:252–256
64. Basile-Doelsch I et al (2005) Another continental pool in the terrestrial silicon cycle. Nature 433:399–402
65. De la Rocha CL et al (2000) A first look at the distribution of the stable isotopes of silicon in natural waters. Geochim Cosmochim Acta 64:2467–2477
66. Ragueneau O, Tréguer P, Leyneart A et al (2000) A review of the Si cycle in the modern ocean: recent progress and missing gaps in the application of biogenic opal as a paleoproductivity proxy. Glob Planet Chang 26:317–365
67. Konhauser KO et al (2009) Oceanic nickel depletion and a methanogen famine before the great oxidation event. Nature 458:750–754
68. Saito MA (2009) Less nickel for more oxygen. Nature 458:714–715

69. Egami F (1975) Minor elements and evolution. J Mol Evol 4:113–120
70. Natl Academy of Sciences (1975) Medical and biological effects of environmental pollutants: nickel. Proc. Natl Acad Sci. Washington, DC
71. Yaroshevsky AA (2006) Abundances of chemical elements in the Earth's crust. Geochem Int 44:54–62
72. Liu L (2004) The inception of the oceans and CO_2-atmosphere in the early history of the Earth. Earth Planet Sci Lett 227:179–184
73. Catling CD, Zahnle KJ (2009) The planetary air leak. Sci Am 300:24–31
74. Aki K (1983) Strong motion seismology. In: Kanamori H, Boschi E (eds) Earthquakes: observation, theory and interpretation. North-Holland Pub. Co, Amsterdam, pp 223–250
75. Padron E et al (2008) Changes in the diffuse CO_2 emission and relation to seismic activity in and around El Hierro, Canary Islands. Pure Appl Geophys 165:95–114
76. Cook DN (2010) Models of the atomic nucleus. Springer, Heidelberg, Dordrecht, London, New York
77. Cook ND, Dellacasa V (1987) Face-centered cubic solid phase theory of the nucleus. Phys Rew C 35(5):1883–1890